DEVELOPMENTAL CHANGES IN AUDITORY BRAINSTEM CIRCUITRY

ANATOMICAL REFINEMENT IN THE PROJECTION FROM THE ANTEROVENTRAL COCHLEAR NUCLEUS TO THE LATERAL SUPERIOR OLIVE

By SAMUEL MOLOT-TOKER, B.Sc.

A Thesis Submitted to the School of Graduate Studies in Partial Fulfilment of the Requirements for the Degree Master of Science

MASTER OF SCIENCE (2015) McMaster University
NEUROSCIENCE Hamilton, Ontario

TITLE: Anatomical Refinement in the Projection from the Anteroventral Cochlear Nucleus to the Lateral Superior Olive

AUTHOR: Samuel Molot-Toker, B.Sc. (McGill University, Montreal, Quebec)

SUPERVISOR: Dr. Deda C. Gillespie

NUMBER OF PAGES: viii, 63

ABSTRACT

In mammals, the basic computations required for azimuthal sound localization are performed by a group of auditory brainstem nuclei known as the superior olivary complex (SOC). The lateral superior olive (LSO), in the SOC, aids in sound localization by computing intensity differences between sounds arriving at the two ears. It does this by comparing excitatory input from the ipsilateral anteroventral cochlear nucleus (AVCN) with inhibitory input from the ipsilateral medial nucleus of the trapezoid body (MNTB), which is driven by the contralateral AVCN. In order for sounds to be accurately localized, the AVCN-LSO and MNTB-LSO projections must be aligned with each other in a frequency-dependent manner. Rough alignment occurs over the course of development, but a significant amount of circuit refinement is required to achieve adult-like precision. Two types of refinement occur in these pathways: 1) physiological, or functional refinement; and 2) anatomical refinement. Little is known about the latter type of refinement in the AVCN-LSO pathway.

In order to study this, I conducted a variety of experiments all aimed at anterogradely labeling a small number of cells projecting from the AVCN to the LSO in juvenile rats. I experimented with several approaches in order to develop the technique of *ex vivo*, sparse axon labeling in this area of the brain. I show the optimal technique developed after testing various tracers, application methods, and incubation times, among others. This optimized technique can now be used in a future experiment that will uncover and describe anatomical refinement in the AVCN-LSO pathway of the auditory brainstem.

ACKNOWLEDGEMENTS

First and foremost, I would like to thank my supervisor, Dr. Deda Gillespie. Deda always encouraged me to push myself just a little bit out of my comfort zone, and I can say with 100% certainty that I am all the better for it. Without her guidance and mentorship over the past two years, I would not have had the confidence or competence to accomplish all that I have, both in and outside the lab.

I am also grateful to the members of my supervisory committee, Dr. Elyanne Ratcliffe and Dr. Laurie Doering, whose input and genuine interest in my research were always appreciated.

Special thanks to all the members of the Gillespie Lab with whom I have crossed paths; specifically, without the help of Dr. Javier Alamilla, Dr. Alan Cooper, and Hugo Wang, there are many times I would have been completely lost.

Finally, I am forever indebted to my friends and family, whose patience and comfort know no bounds. There were days when I did not make it easy, to be sure, but they always gave me the benefit of the doubt. Without their love and support, none of this would have been possible. Thank you.

TABLE OF CONTENTS

LIST OF FIGURES AND TABLES

LIST OF ABBREVIATIONS

ACSF	artificial cerebrospinal fluid
AMPA	α-amino-3-hydroxy-5-methyl-4-isoxazolepropionic acid
ATP	adenosine triphosphate
AVCN	anteroventral cochlear nucleus
CF	characteristic frequency
CNC	cochlear nuclear complex
DCN	dorsal cochlear nucleus
E#	embryonic day #
(E)PSP	(excitatory) postsynaptic potential
GABA	γ-aminobutyric acid
GBC	globular bushy cell
IC	inferior colliculus
ILD	interaural level difference
IPD	interaural phase difference
ITD	interaural time difference
KCC2	potassium-chloride cotransporter 2
LSO	lateral superior olive
MNTB	medial nucleus of the trapezoid body
MSO	medial superior olive
MW	molecular weight
NA	numerical aperture
NMDA	N-methyl-D-aspartic acid
NR2B	NMDA receptor subunit 2B
P#	postnatal day #
PBS	phosphate-buffered saline
PVCN	posteroventral cochlear nucleus
SBC	spherical bushy cell
SOC	superior olivary complex
VCN	ventral cochlear nucleus
VGLUT3	vesicular glutamate transporter 3

DECLARATION OF ACADEMIC ACHIEVEMENT

I designed all of the experiments described herein with Dr. Deda Gillespie. I independently conducted all of the procedures, from animal breeding to data collection. My colleague, Hugo Wang, designed and implemented the custom electroporation circuit briefly mentioned in Section 2.7.

1. Introduction

1.1 Sound localization and sensation

In the animal kingdom, accurate sound localization is of critical importance in predator-prey dynamics and communication with conspecifics. As humans, we rarely find ourselves in the former situation, and yet, because we are such social animals, sound localization is equally indispensable in our daily lives. Besides the obvious difficulties one would experience without being able to accurately localize sounds, subtler handicaps would arise, such as the loss of the ability to follow specific conversations in noisy environments (also known as the cocktail party effect), for example. In mammals, the superior olivary complex (SOC), a group of brainstem nuclei, is the first site of binaural information processing, and is essential for the localization of sound along the azimuth, or horizontal plane. The various nuclei of the SOC accomplish this feat by integrating and comparing different features of sound stimuli as they arrive at the two ears. Some nuclei of the SOC respond best to temporal cues, such as interaural time and phase differences (ITDs and IPDs, respectively), while others respond best to sound intensity cues, like interaural level differences (ILDs). In the SOC, the medial superior olive (MSO) is the nucleus that primarily computes ITDs (Masterton and Diamond 1967; Masterton et al. 1975; Yin and Chan 1990), and the lateral superior olive (LSO) is the nucleus that primarily computes ILDs (Boudreau and Tsuchitani 1968). ITDs occur because it takes a fraction of a millisecond longer for sound to reach the ear farther from a sound source, whereas ILDs are largely the result of an “acoustic shadow” cast by the animal’s head

when sound waves are reflected off its surface (Grothe et al. 2010). Which mechanism is used to localize a sound depends on the frequency of that sound: ITDs are only used for lower frequencies, while ILDs are only used for higher frequencies. The reason for this dichotomy is that ITDs and IPDs for high frequency sounds are very difficult to detect, due to the fact that numerous small waveforms occur in the short distance between the ears, while ILDs for low frequency sounds are similarly imperceptible, because the longer wavelengths simply bend around the head. The switch between the two mechanisms, therefore, occurs in the range of frequencies where the distance between the ears is approximately half as long as the wavelength of the sound. For humans, that range of frequencies is theoretically centred around 1 kHz (personal calculation). When the auditory system is presented with sounds that fall in this range, it relies on a combination of ambiguous ITDs and weak ILDs to localize them. Psychophysical studies in humans have in fact shown that our ability to localize these mid-frequency sounds suffers due to the transition between the dual mechanisms (Tollin 2003). In light of this, some species have evolved to rely more on the LSO than on the MSO for localizing sounds, or vice versa. This strongly depends on the audible frequency range of that species, as shaped by evolutionary forces. Cats, for example, have a very well-developed MSO and perform well in low frequency localization tasks (Masterton et al. 1975). Rats, on the other hand, have a relatively underdeveloped MSO (Harrison and Irving 1966c) and perform poorly in the same task (Masterton et al. 1975). The unique circuitry of the SOC takes advantage of these aforementioned phenomena, using them to lay the foundations for an auditory map of the external environment.

The auditory system must rely on such computations to extrapolate the physical position of auditory stimuli because the cochlea provides no such information on its own. This is in direct contrast to the sensory epithelium of the visual system, the retina, which directly encodes a neural representation of visual space. This neural map of visual space, called the retinotopic map, is replicated throughout the central visual system. It is organized such that neighbouring neurons respond to, or represent, adjacent areas in visual space. The retinotopic map is a specific example of a common type of cellular organization known as neural topography. Neural topography is found in all five classical mammalian sensory systems (e.g. Sperry 1963, visual; Boudreau and Tsuchitani 1968, auditory; Killackey et al. 1995, somatosensory; Auffarth 2013, olfactory; Chen et al. 2011, gustatory). It results in the formation of topographic maps throughout the central nervous system, in both cortical and subcortical structures. Just like the retinotopic map, other topographic maps are arranged such that neighbouring neurons respond to physically similar stimuli in either a continuous (as in the visual, auditory, and somatosensory systems) or discrete (as in the olfactory and gustatory systems) manner (Luo and Flanagan 2007). As implied earlier, neighbouring neurons in the cochlea do not respond to neighbouring areas in auditory space; instead, they respond to neighbouring frequencies in the audible spectrum. Appropriately, individual neurons in these maps exhibit a characteristic frequency (CF) to which they respond best (e.g. Boudreau and Tsuchitani 1968), and neurons with similar CFs are arranged into isofrequency bands. This subtype of neural topography, known as cochleotopy or tonotopy, is introduced into

the auditory system by the basilar membrane of the cochlea, and is preserved all the way up to the auditory cortex (Saenz and Langers 2014).

In order to appreciate the ontogeny of the tonotopic map, one must first understand how auditory stimuli are neurally encoded. When sound waves reach the eardrum, they are mechanically amplified and transduced into physiological pressure waves by the three bones of the inner ear. These waves travel through the perilymph of the cochlea, where different parts of the basilar membrane are deflected in response to the various component frequencies of the original sound: The stiff base of the basilar membrane responds to higher frequencies, while the more flexible apex responds to lower frequencies. In this fashion, the entire audible range of frequencies is represented continuously and logarithmically on the basilar membrane (Hudspeth 2013). This unique characteristic is what produces tonotopy within the auditory system. The vibrations along the basilar membrane trigger receptor potentials in different groups of inner hair cells along the coiled length of the cochlea. The inner hair cells then convey their electrical activity to the type I neurons of the spiral ganglion, whose axons make up around 95% of the auditory portion of the eighth cranial nerve (Brown and Santos-Sacchi 2008). Finally, the auditory nerve fibres conduct the information to the cochlear nuclear complex (CNC), all the while maintaining tonotopic organization.

1.2 Auditory brainstem anatomy and general connectivity

The CNC is the gatekeeper to rest of the central auditory pathway, and therefore plays a crucial role in sound localization circuitry. It comprises the dorsal cochlear

nucleus (DCN) and the ventral cochlear nucleus (VCN). The latter can be further divided into the anteroventral cochlear nucleus (AVCN) and the posteroventral cochlear nucleus (PVCN), which are classically delineated by the bifurcation of the auditory nerve fibres into ascending and descending branches, respectively (Ramón y Cajal 1909; Harrison and Irving 1965). Although the actual boundary between the AVCN and PVCN has been brought into question more recently (e.g. Harrison and Irving 1996b; Osen 1969; Webster and Trune 1982), the DCN is indisputably separate, featuring a distinct layered cytoarchitecture and a complex intrinsic connectivity (Webster and Trune 1982; Cant and Benson 2003). Each of the three subdivisions of the CNC features its own tonotopic axis, but they are all oriented in approximately the same direction: High frequencies are represented dorsomedially, while low frequencies are represented ventrolaterally (colour gradients in Figure 1) (Friauf 1992; Luo et al. 2009). Across all species studied thus far, the gross morphology and general divisions of the CNC appear to be fairly consistent (Webster and Trune 1982); species differences arise, however, under closer scrutiny. This natural variance, combined with the historical use of different staining protocols and neuronal classification criteria, has resulted in nearly as many differing schematics of the nucleus as there are studies on the matter. For example, in a classic study on the CNC of cats, Osen (1969) concluded that the VCN could be further divided into five regions according to the distribution of cell types she observed following Nissl and reduced silver stains. Brawer et al. (1974), on the other hand, identified 13 unique cellular areas in the VCN of cats, based on conglomerated data from Nissl, reduced silver, and Golgi stains. While there may be some disagreement on the neuronal classification and the parcellation

of the CNC – both between and within species – the general connectivity is remarkably consistent (for review, see Cant and Benson 2003). Most of the numerous neuron types within the DCN do not project outside the CNC, resulting in an intricate intrinsic circuitry; those that do, however, project primarily to the inferior colliculi (IC) and the contralateral CNC. Since the output of the DCN circumvents the SOC, it will no longer be considered in this review. Conversely, the primary efferents of the PVCN and the AVCN directly target the SOC.

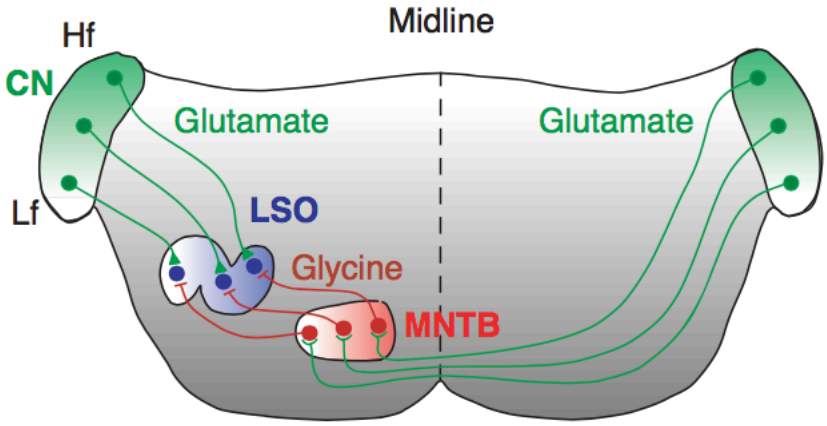

Figure 1. Connectivity and tonotopicity in the rat auditory brainstem. (from Kandler and Gillespie 2005)

The three major nuclei of the SOC are the LSO, the MSO, and the medial nucleus of the trapezoid body (MNTB). As alluded to earlier, the cells of each nucleus are organized tonotopically (colour gradients in Figure 1). In the rat LSO, the frequency gradient decreases in the dorsomedial to ventrolateral direction (following the S-shape of the nucleus), while in the MNTB, the same gradient is simply expressed mediolaterally

(Friauf 1992). The cells of the LSO receive two main inputs: an excitatory, glutamatergic input from the ipsilateral AVCN, and an inhibitory, glycinergic input from the ipsilateral MNTB (Figure 1) (Moore and Caspary 1983; Cant 1984; Sanes et al. 1987; Bledsoe et al. 1990; Glendenning et al. 1991). The MNTB is a sign-inverting nucleus that receives a high-fidelity glutamatergic input from the contralateral VCN (Harrison and Warr 1962; Harrison and Irving 1966b). Accordingly, the LSO of each hemisphere is excited by respectively ipsilateral sounds, and inhibited by contralateral ones. At the cellular level, the converging inputs of opposite signs are integrated in a simple, additive manner: An LSO cell will fire if an ipsilaterally-presented sound is louder than the same sound presented simultaneously to the contralateral ear; conversely, an LSO cell will be inhibited if the intensity of a contralaterally-presented sound is equal to, or greater than that of the same sound presented ipsilaterally (Boudreau and Tsuchitani 1968; Moore and Caspary 1983).

In order for the LSO to accurately compute ILDs, the converging excitatory and inhibitory inputs must be tonotopically aligned. Exactly how this occurs is an important question in the field that has yet to be answered. Before we can address this, however, we must first understand the development and refinement of the two individual inputs to the LSO (see Section 1.4). The term "refinement," in this context, refers to the activity-dependent neural plasticity that occurs during a critical developmental period in the animal's early life. Discussions on development, plasticity, and refinement are meaningless, however, without first discussing the very cells in which these processes are occurring.

1.3 Cell morphology and organization

While many different cell types have been identified in the VCN, those of greatest relevance to this thesis are the spherical bushy cells (SBCs) and, to a lesser extent, the globular bushy cells (GBCs). SBCs are glutamatergic (Cant 1984, Glendenning et al. 1991) neurons found primarily in the most rostral part of the AVCN, appearing less frequently in the more caudal regions (Harrison and Irving 1965, rat; Osen 1969, cat; Brawer et al. 1974, cat; Hackney and Pick 1986, guinea pig). The primary inputs received by SBCs are the large, excitatory endbulb of Held synapses from the ascending branches of the auditory nerve fibres (Ramón y Cajal 1909; Harrison and Irving 1965). SBC axons exit the AVCN via the trapezoid body and terminate in the ipsilateral LSO, the lateral part of the ipsilateral MSO, and the medial part of the contralateral MSO (Harrison and Irving 1965, 1966a; Cant and Casseday 1986). In the LSO, the round vesicle-containing (i.e. glutamatergic) terminals of SBCs form synapses primarily with the distal dendrites of principal cells (Cant 1984).

GBCs are also glutamatergic (Guinan and Li 1990) neurons; however, they are found in the more posterior aspect of the AVCN, as well as in the anterior aspect of the PVCN (Harrison and Irving 1966b; Hackney et al. 1990). Like the SBCs, they too receive their primary inputs from ascending auditory nerve fibres, but the synapses are not quite as large as the endbulbs of Held found on the former cell type (Harrison and Irving 1966b). The large diameter axons of GBCs exit the VCN via the trapezoid body and continue along the ventral border of the brainstem, crossing midline to reach the contralateral MNTB (Harrison and Warr 1962; Harrison and Irving 1966b; Smith et al.

1991). Once in the MNTB, GBCs terminate in specialized structures known as the calyces of Held (Ramón y Cajal 1909; Harrison and Warr 1962; Smith et al. 1991). These axon terminals practically engulf the postsynaptic cell somata, making them the largest known synapses in the mammalian brain.

As the targets of SBCs, it is important to understand the morphology and organization of LSO cells. Rietzel and Friauf (1998) identified seven distinct cell types within the rat LSO. This is several more than had been identified in other species, but the authors attributed this to methodological limitations of those other studies (see Helfert and Schwartz 1986, cat; and Helfert and Schwarz 1987, gerbil). Of the seven cell types, the authors propose that three fall into the category of "principal cells," according to criteria established in studies of other species: bipolar cells, banana-like cells, and unipolar cells. These three cell types share several commonalities, but also exhibit some important differences: First, all three cell types have relatively large, fusiform somata. Second, the dendritic branching patterns of the three cell types are fairly consistent across all ages studied. Additionally, all of the cells feature primary dendrites that project from polar ends of the somata – with the exception of unipolar cells, as they typically only have one primary dendrite. The dendritic trees are all generally oriented approximately perpendicular to the tonotopic gradient (i.e. the S-axis) of the nucleus, as well. A significant difference, however, is found in the distribution of the different cell types within the nucleus: Bipolar cells are only found in the medial half of the LSO, while banana-like cells are only found in the lateral half. This observation may provide a clue as to the functional differences between the different principal cell types. While it is well

established that the LSO sends a primarily glutamatergic projection to the contralateral IC (Glendenning et al. 1992; Ito and Oliver 2010), and a primarily glycinergic projection to the ipsilateral IC (Saint Marie et al. 1989; Glendenning et al. 1992), it remains unclear which principal cell types belong to which group. Interestingly, Glendenning and Masterton (1983; further explored in Glendenning et al. 1992) noted that contralaterally projecting LSO cells are mainly confined to the medial limb of each nucleus, whereas ipsilaterally projecting cells are found more in each lateral limb. Considering this information, it is possible that the more medial bipolar cells of Rietzel and Friauf (1998) are glutamatergic cells that project to the contralateral IC, while the more lateral banana-like cells are glycinergic cells that project to the ipsilateral IC. The function of unipolar cells – and the other cell types, for that matter – remains unclear (see conflicting statements in Rietzel and Friauf (1998): "No bipolar cells were identified in the lateral limb of the LSO (although… unipolar, and banana-like cells were found here; …)" [p. 22] and "Like bipolar cells, unipolar cells were never seen in the lateral limb of the LSO." [p. 25]).

1.4 Circuit development and refinement

The sound localization circuitry is established during a developmental period that encompasses late embryonic and early postnatal days. This is followed by a necessary period of refinement, in which the immature circuitry becomes more precisely tuned, and adult-like in functionality. This critical developmental period begins around one week before birth in rats, when efferent projections from the CNC start to invade the auditory

brainstem (Kandler and Friauf 1993). This period consists exclusively of axonal outgrowth, and persists until embryonic day 17 (E17). On E18, Kandler and Friauf (1993) noted the first axon collaterals beginning to innervate their eventual target nuclei. Collateral branching continues through birth, which occurs on E22, and well into the first postnatal week. By postnatal day 5 (P5), the adult innervation pattern of the CNC efferents has been achieved; however, this does not mark the end of development. Starting at P5, axon terminals begin to mature, and specialized structures, such as the calyces of Held, begin to develop. This period of development continues until about P14. This is slightly after the onset of hearing in rats, which are altricial animals, and therefore deaf for the first two postnatal weeks (inner hair cell activity can be detected by P12, with small auditory brainstem responses detectable by P14; Blatchley et al. 1987). Even in the absence of sound-evoked activity, and therefore relying solely on gradients of axon guidance molecules and spontaneous activity (Cramer 2005; Tritsch et al. 2007), the formation of this circuitry is remarkably accurate; consequently, Kandler and Friauf (1993) were unable to find any significant instances of aberrant projections (i.e. to the ipsilateral MNTB or contralateral LSO) in their experiments. Ectopic projections from the VCN can be induced, however, following unilateral cochlear ablation just after birth (Kitzes et al. 1995). Under this condition, the VCN contralateral to the cochlear ablation not only innervates the appropriate nuclei, but also sends axons to the ipsilateral MNTB, the contralateral LSO, and the distal halves of each MSO. Interestingly, although the projections themselves are inappropriate, they still project to the correct tonotopic

positions within each nucleus, and the synapses are highly functional well into adulthood (Kitzes et al. 1995).

As for the development of functional synapses in the SOC circuitry, Kandler and Friauf (1995) were able to record both ipsilaterally and contralaterally evoked postsynaptic potentials (PSPs) as early as E18 in acute brainstem slices containing rat LSO. At this age, however, PSPs are subthreshold; action potentials can only be elicited from E20 onward (Kandler and Friauf 1995). In the following two weeks, the latencies and durations of both ipsilaterally and contralaterally evoked PSPs become shorter, signifying a maturation of synaptic transmission. All of these changes occur before hearing onset, and are therefore driven purely by spontaneous activity in the system.

While the VCN efferents are developing, their target cells in the various nuclei of the SOC are also developing. In addition to identifying the different cell types of the rat LSO, Rietzel and Friauf (1998) characterized the developmental changes that occur in bipolar cell morphology. These changes, also known as anatomical refinement, are essential for proper circuit function. From P4 to P36, there is no appreciable change in the size of bipolar cell somata. The same cannot be said, however, for their dendritic arbours. First, the number of primary dendrites decreases from as many as 15 at P4, to as few as 2 by P36. Due to this, as well as the pruning of most distal branches, bipolar cells lose approximately 80% of their dendritic endpoints in the first postnatal month. While most endpoints are lost during this time, the absolute size of the dendritic field still increases with age. Interestingly, the relative size of the dendritic field in the LSO actually decreases slightly, due to a disproportionate increase in the size of the LSO at this

developmental stage. Overall, the dendritic fields become narrower along the tonotopic axis of the LSO, resulting in more precisely tuned auditory responses. The most dramatic changes in this refinement process occur between P4 and P15, meaning that this period of drastic dendritic refinement mostly occurs in the absence of experience-dependent (i.e. sound-evoked) activity. That said, spontaneous neural activity, as mentioned earlier, has been observed in the developing auditory system (Gummer and Mark 1994; Lippe 1994; Tritsch et al. 2007), and it undoubtedly has an effect on SOC circuit development and refinement (Clause et al. 2014), just as spontaneous retinal activity affects the developing visual pathway (Galli and Maffei 1988; Shatz and Stryker 1988; Maffei and Galli-Resta 1990; Meister et al. 1991; Wong et al. 1993; Triplett et al. 2009).

Occurring at the same time as the dendritic refinement in the LSO, is the complementary refinement of the axonal arbours of MNTB and AVCN neurons terminating in the LSO. Due to the fact that the MNTB-LSO pathway is relatively large, strictly inhibitory (in adults; see below), and precisely (i.e. tonotopically) organized, it is an attractive model in which to study inhibitory synapse development and refinement. The AVCN-LSO pathway, on the other hand, appears, at least superficially, to be just like any other topographically organized excitatory projection. This has resulted in a strong bias in favour of conducting research in the former pathway over the past few decades. As such, considerably more is known about the development and refinement of the MNTB-LSO pathway than of the AVCN-LSO one.

Although adult MNTB principal cells are considered to be glycinergic (e.g. Bledsoe et al. 1990), they do not begin their lives as such. For the first two postnatal

weeks in rodents, immature MNTB cells actually release more GABA than glycine (Kotak et al. 1998; Nabekura et al. 2004). Furthermore, during the first postnatal week, MNTB cells also release glutamate (Gillespie et al. 2005). This occurs during a time in which VGLUT3 – a vesicular glutamate transporter found in typically non-glutamatergic synapses (Fremeau et al. 2002) – is expressed in the SOC (Blaesse et al. 2005). In addition to the excitatory action of glutamate released from these immature MNTB cells, GABA and glycine are actually depolarizing (Kandler and Friauf 1995; Ehrlich et al. 1999) and excitatory (Kullmann and Kandler 2001) during the same timeframe. The typically hyperpolarizing neurotransmitters are depolarizing at this age because of the abnormally high intracellular Cl^- concentrations in LSO cells (Ehrlich et al. 1999; Becker et al. 2003). This results in a net efflux of Cl^- when ionotropic GABA or glycine receptors are activated, thereby depolarizing the postsynaptic membrane. Therefore, at this young age, stimulation of LSO cells via the MNTB will trigger Ca^{2+}-signalling pathways and other downstream effects typically associated with action potentials and excitatory neurotransmission (Friauf 1993; Kullmann et al. 2002). Given these findings, Kandler and Gillespie (2005) proposed the following model to explain how synaptic plasticity could occur at these developing inhibitory synapses: The release of GABA and glycine, during a time when these neurotransmitters are depolarizing, could alleviate the Mg^{2+} blockage of NMDA receptors present at, or near the synapse (Case and Gillespie 2011), allowing the co-transmitted glutamate to then activate these receptors. Ultimately, this would lead to the insertion of more GABA and/or glycine receptors into the postsynaptic membrane, thus strengthening the inhibitory nature of the synapse. As the LSO cells mature, KCC2, a

K^+-Cl^- cotransporter that is present, but inactive in immature LSO cells, becomes active (either by insertion into the membrane or some other post-translational modifications), thus lowering internal Cl^- concentrations (Becker et al. 2003; Balakrishnan et al. 2003; Löhrke et al. 2005). Consequently, activation of ionotropic GABA and glycine receptors then results in a net influx of Cl^-, thereby hyperpolarizing the cells.

Likely as a direct result of these distinct changes occurring in both MNTB cells and LSO cells, some other notable changes occur in the MNTB-LSO pathway itself. In the first two postnatal weeks, individual LSO cells lose approximately 75% of their MNTB inputs (Kim and Kandler 2003). At the same time, however, the remaining synapses experience at least a 12-fold increase in conductance (Kim and Kandler 2003), likely due to increases in both the quantal size (i.e. the synaptic response to the release of a single vesicle) and quantal content (i.e. the number of vesicles released following stimulation) (Kim and Kandler 2010). This synaptic elimination and strengthening is known as functional refinement, and is driven by spontaneous activity in the developing auditory system, since the changes largely occur before hearing onset.

The MNTB-LSO pathway also experiences anatomical refinement. In contrast to functional refinement, anatomical refinement in this pathway occurs primarily after hearing onset, when the circuitry is being driven by experience-dependent, rather than spontaneous, activity. Sanes and Siverls (1991) documented these anatomical changes in MNTB neurons during the first three postnatal weeks in gerbils. While some degree of tonotopic alignment is indeed present even at young ages (P2-3), there is a marked narrowing of the axonal arbours along the tonotopic axis of the LSO as the animals

mature. Although the most significant changes occur after hearing onset, entire branches projecting to inappropriate isofrequency bands are eliminated during the first two postnatal weeks (i.e. before hearing onset). Furthermore, both the spread and number of terminal boutons in the LSO decrease significantly from around hearing onset to P18-25. In a later study, Sanes and Takács (1993) investigated the effects of cochlear ablation on the anatomical refinement in this pathway. Unilateral cochlear ablation effectively denervates the contralateral MNTB, depriving it of any experience-dependent activity. In these denervated animals, the spread and number of MNTB-LSO terminal boutons were considerably higher than in control animals. Additionally, the axons of experimental animals featured more branching points than normal, and the general orientations of the axonal arbours typically were not perpendicular to the tonotopic axis of the LSO. Overall, a lack of concerted circuit activity at this critical developmental stage results in a persistent immature state.

Refinement in the AVCN-LSO pathway is less well-characterized. Regarding functional refinement, Case et al. (2011) found that elimination and strengthening of synapses also occurs in this pathway, but to a lesser degree than in the MNTB-LSO pathway. Furthermore, these changes occur during the first two postnatal weeks, just like the similar processes in the MNTB-LSO pathway. During this time, the relative contribution of NMDA receptors to the excitatory PSPs (EPSPs) decreases, while the contribution of AMPA receptors increases (Case et al. 2011). Moreover, the remaining NMDA receptor-mediated component of the EPSPs becomes less sensitive to ifenprodil with age. Ifenprodil is a selective antagonist of the NR2B subunit of NMDA receptors, a

subunit typically associated with immature synapses (Case et al. 2011). Taken together, these findings clearly show that the maturation and strengthening of AVCN-LSO synapses occurs in a timeframe that mirrors the functional refinement of MNTB-LSO synapses.

Currently, nothing is known of the anatomical refinement that takes place in the AVCN-LSO pathway; however, given that functional refinement in the two pathways occurs simultaneously, it is fair to assume that anatomical refinement would also follow a similar timecourse. Unfortunately, this has yet to be confirmed. Without knowing if, when, or to what extent refinement occurs in this individual pathway, we cannot begin to uncover the mechanisms underlying the remarkable alignment between the two converging inputs.

2. Research methodology

2.1 Introduction

In order to characterize the timecourse and extent of anatomical refinement in the axonal arbours of the AVCN-LSO pathway, I sought to label a small number of SBCs with an anterograde tracer, to later be imaged and reconstructed in three dimensions for subsequent analysis. My research and findings helped elucidate the optimal technique and parameters required to successfully complete such a project. Over the course of my time on this project, I experimented with different tracers, different directions of approach and points of entry into the AVCN, different means of introducing those tracers into the AVCN, and different incubation times and conditions. After a description of the animal

subjects used in my experiments, I provide a general outline of my most recent, and most successful, experimental protocol. Following this is an overview of how this protocol came to be, including any major variations I tried, or significant parameters I changed, in an effort to improve my results.

2.2 Animal subjects

All animal procedures were approved by McMaster University's Animal Research Ethics Board, and adhered to the standards and guidelines outlined by the Canadian Council on Animal Care. Since this research project is of a developmental nature, the experiments were conducted in animals of different ages. Sprague Dawley rats (Charles River Laboratories) aged P3, P12, and P21 were used in these experiments, with no discrimination made between sexes (Ehmann et al. 2008). Of the 126 animals used in my experiments, only 5 were from the younger age group, and only 7 were from the older one. Being so young and small, the P3 animals were significantly more difficult to work with than the older ones. Conversely, the brains of P21 animals required longer incubation times and took longer to image because they were so much bigger than P12 brains. Therefore, I chose to conduct most of my experiments in P12 animals until the technique was perfected. These three age groups were deliberately chosen to reflect distinct developmental stages in the animals: At P3, well before hearing onset in rats, the SOC circuitry is relatively immature, yet in a state of rapid development. Nine days later, at P12, the rats are just starting to hear for the first time. Prior to this, it is only spontaneous activity driving all the changes in the circuitry; therefore, the onset of sound-

evoked activity in the SOC circuitry marks a significant developmental landmark. Another nine days after this, at P21, the SOC circuitry is approaching a mature state, but anatomical refinement is still occurring slowly (Sanes and Siverls 1991). By analyzing the branching patterns of axonal arbours across these three evenly-spaced, distinct developmental stages, we could paint a picture of anatomical refinement in the AVCN-LSO pathway.

2.3 Final experimental protocol

To begin each experiment, animals were anaesthetized with isoflurane and decapitated. Brains were then quickly removed and immediately placed into a beaker of oxygenated artificial cerebrospinal fluid (ACSF, pH 7.2; containing, in mM: 124 NaCl, 1.3 $MgSO_4 \cdot 7H_2O$, 5 KCl, 1.25 KH_2PO_4, 10 dextrose, 26 $NaHCO_3$, 2 $CaCl_2 \cdot 2H_2O$, 0.4 ascorbic acid, 3 myoinositol) in order to wash off any excess blood prior to introducing the neuronal tracer into the tissue. Brains were then transferred to a shallower dish filled with agar, and secured in place, ventral side up, using 30-gauge needle tips pinned bilaterally in the cerebral cortices (i.e. far from the brainstem). A pipette filled with fresh, recently oxygenated ACSF was used to ensure that the brains never dried out during the staining procedure.

Prior to sacrificing the animals, a solution containing the neuronal tracer was made and loaded into freshly-pulled borosilicate glass microelectrodes (1-2 MΩ; Model P-97 Micropipette Puller, Sutter Instrument Co.). With the ventral surface of the brain exposed, the AVCN was easy enough to locate with nothing more than a low-power

dissecting microscope. Using a manual micromanipulator, the tip of the microelectrode was lowered to the surface of the AVCN and then inserted into the nucleus to a depth of at least 10 μm. With the microelectrode in the target nucleus, the tracer was injected with one or two pressure pulses from a picospritzer (Picospritzer II, Great Valve Corporation), followed by a variable train of electrical stimuli from an intracellular amplifier (Model 1600 Neuroprobe Amplifier, A-M Systems Inc.) gated by a square-wave stimulator (S48 Square Pulse Stimulator, Grass Technologies). The stimulus train was used to encourage the uptake of tracer by the cells of the AVCN, via a process known as electroporation (see Section 2.6).

Following the tracer injections and electroporation, brains were placed into a large beaker of fresh, continuously oxygenated ACSF to incubate for 4-5 hours while the tracer was transported from the injection site in the AVCN to the axon terminals in the LSO. Following the incubation period, brains were fixed in 4% paraformaldehyde in phosphate-buffered saline (PBS, pH 7.4) at 4°C for around 24 hours, and then cryoprotected in a solution of 30% sucrose in PBS at 4°C for at least 18 hours. Once the brains had sunk to the bottom of their vials, indicating the completion of cryoprotection, they were sliced at 50 μm on a freezing microtome. The collected sections always covered the entirety of the LSO, as well as the more rostral part of the AVCN whenever possible (to see the injection site). Sections were mounted onto gelatin-subbed slides, and then coverslipped with homemade gelvatol (a polymerizing, aqueous mounting medium). Finally, sections were imaged on a laser scanning confocal microscope (Nikon D-Eclipse C1) with a 40x oil-immersion objective (1.3 NA).

2.4 Parameterization #1: Location and direction of tracer application

Since the population of neurons in the CNC is so heterogeneous, it was important to apply or inject the tracer in such a way as to maximize the probability of labeling SBCs, rather than another cell type. In an effort to optimize this probability, I experimented with different rostrocaudal injection sites, and different directions of approach. Injections were always made in the rostral half of the visible part of the CNC (i.e. the AVCN), but within that rostral half I experimented with finer positioning. I also tried approaching the nucleus rostrally, medially, and laterally. Each approach had its own theoretical benefits: Approaching the AVCN rostrally would likely maximize the probability of labeling SBCs, because they are mostly found towards the anterior pole of the AVCN; approaching medially seemed beneficial due to the fact that the microelectrode would pass through the trapezoid body (i.e. the fibre tract through which SBC and GBC axons travel to reach their targets), thereby increasing the amount of tracer introduced into the proximal axons; finally, approaching laterally provided the best maneuverability and access to the AVCN. I did not attempt a caudal approach, because that risked labeling more caudal-lying cells, like GBCs and other cells of the PVCN or DCN.

2.5 Parameterization #2: Tracer selection

I experimented with three different tracers in an effort to optimize the results of my research: biocytin, a 10,000 molecular weight (MW) dextran (Alexa488D; Invitrogen), and a 3000 MW dextran (micro-ruby; Invitrogen).

Biocytin is a lysine-conjugated form of biotin (or vitamin H), which is naturally found in neurons. Due to its high affinity to avidin and chemically similar derivatives, biocytin can be visualized in a number of ways; we used fluorophore-conjugated streptavidin. To this end, biocytin-treated brains were fixed, cryoprotected, and sliced (see Section 2.3), and then free-floating sections were incubated in a 1:1000 dilution of DyLight 549-conjugated streptavidin (Jackson ImmunoResearch) in PBS, plus 0.5% Triton X-100, overnight at 4°C.

Dextrans are much less membrane-permeant than biocytin (Barker et al. 2009), meaning that alternative methods were required to introduce them into the cells of the AVCN (see Section 2.6, below). Furthermore, the dextrans I used are conjugated to visible dyes, which eliminates the necessity for subsequent histological staining. Alexa488D, as the name suggests, is conjugated to the Alexa Fluor 488 dye, while micro-ruby is conjugated to tetramethylrhodamine.

2.6 Parameterization #3: Tracer application method

In the very first experiments, rather than injecting a biocytin solution into the AVCN, I simply implanted small crystals of biocytin into the nucleus (as per Kandler and Friauf 1993). The crystals I used were as small as possible, just barely visible to the naked eye. They were picked up on the tips of fine metal microelectrodes, and implanted into the AVCN after its surface was quickly dabbed dry with tissue paper (to ensure the crystals did not dissolve into solution prior to reaching the desired tissue depth). For many experiments, I pierced both AVCNs of one brain without picking up a new biocytin

crystal. This was done in an effort to further limit the amount of tracer being introduced into the tissue, because the smaller crystals I intended to use often fell off the microelectrode before they could be implanted.

In subsequent experiments, instead of implanting solid crystals, I iontophoretically ejected or pressure-injected a 4% solution of biocytin, Alexa488D, or micro-ruby in PBS. For these experiments, hollow glass micropipettes were used instead of metal microelectrodes. That said, the glass micropipettes were threaded with silver wire to make them microelectrodes as well. This was necessary in order to carry out the electroporation required to induce the uptake of dextrans into the SBCs.

As mentioned above, dextrans are impermeant to biological membranes, and therefore require assistance to enter cells. Electroporation, as the name suggests, is the process by which electrical stimulation is used to disrupt biological membranes, thereby opening transient pores through which normally impermeant molecules can enter cells (Barker et al. 2009). The technique was developed as a less harmful, and more efficient alternative to chemically or virally transfecting cells with DNA plasmids (for review, see Escoffre et al. 2009). While electroporation is classically associated with genetic manipulations, it has more recently been used to fill cells with relatively large dyes and tracers, like fluorophore-conjugated dextrans (Haas et al. 2002; Barker et al. 2009).

With the glass microelectrodes filled with tracer solution, electroporation was initiated under the control of either the Grass S48 stimulator alone, or the stimulator and the Neuroprobe intracellular amplifier together. The latter machine features more sensitive electronics that make it better suited to finer-scale electroporation techniques

(described below). Using the stimulator, trains of constant-voltage, square-wave pulses could be delivered to the tissue. Given the many adjustable parameters on the stimulator, these pulse trains could be configured in a nearly infinite number of ways. When used in conjunction with the intracellular amplifier, the customizable protocols of the stimulator temporally gated the current pulses of the amplifier. In finding the best stimulating protocol for my experiments, I started by consulting the literature for studies employing electroporation for purposes similar to my own. In a study on the connectivity of the avian auditory brainstem, Burger et al. (2005) used electroporation to induce the uptake of fluorophore-conjugated dextrans in a relatively large number of cells. They accomplished this with a brief series of three high-amplitude (50 V), low-frequency (10 Hz) pulse trains. With this stimulating protocol, Burger et al. (2005) labeled hundreds of cells – far too many for my purposes. More recently, Ford et al. (2009) used the very same protocol to label GBCs in the gerbil VCN, in an effort to track the development of the ensuing calyces of Held. These authors also labeled hundreds of cells, but they importantly validated the use of the technique in the mammalian brainstem.

On the other end of the spectrum is the work on single-cell electroporation by Rae and Levis (2001). While I was not initially striving for quite that level of precision, the single-cell approach is much more relevant to my project than the alternative, large-scale electroporation. Furthermore, Rae and Levis (2001) outlined some of the guiding principles behind electroporation. According to them, while the exact biochemical mechanisms underlying the phenomenon remain speculative, several things are known to be true: 1) Electroporation is caused by voltage changes near the membrane, not applied

current; 2) the minimum voltage required to open a pore is less than 1 V, with higher voltages producing larger, not more, pores; and 3) voltage pulses lasting less than 1 μs are sufficient to open pores. In their own investigation on the matter, Rae and Levis (2001) found that the success of their electroporation experiments, as measured by gene transfection rates, increased with increasing voltage (to a maximum of about 10 V), as well as with the increasing product of the pulse length and the stimulus frequency. One caveat with the study of Rae and Levis (2001), however, is that their microelectrodes were nearly cell-attached, which is technically more difficult than the protocol of Burger et al. (2005). Given this, I decided to implement a protocol that borrowed elements from both studies. I used the more conservative stimulating protocol of Rae and Levis (2001), so as not to label hundreds of cells as Burger et al. (2005) had, except with less care regarding the placement of the microelectrode, as per the latter group. After many iterative trials, I settled on the following protocol: 100 ms train duration, 500 Hz pulse frequency, 1 ms pulse duration, and 5 V pulse amplitude. Since that protocol is very close to what Rae and Levis (2001) used in single-cell electroporations, but I wanted to label a few more cells than that, I stimulated the nuclei five to ten times using this protocol.

2.7 Parameterization #4: Incubation times and conditions

The distance from the AVCN to the LSO is a relatively long one, with respect to the scale of a neuron; as such, tracer molecules can take a significant amount of time to travel from the point of entry (at the soma) to the axon terminals, especially if passive diffusion is the only means of transport through the cell. Ideally, incubation times should

be maximized in order to allow the tracer to reach the most distal axonal branches; in reality, however, with increasing incubation times comes increasing rates of cell death and degeneration. Therefore, in order for my experiments to be successful, incubation times had to be optimized, as well as incubating conditions that slow apoptotic processes.

To this end, I conducted a set of experiments with gradually increasing incubation times in order to determine when visible tissue degradation commenced. The shortest amount of time the brains were incubated for was three hours, and the longest was nine hours. In addition to this manipulation, I experimented with different temperatures for the oxygenated ACSF bath in which the brains were incubated. Since enzymatic processes and other chemical reactions are strongly governed by temperature, I thought that lowering the temperature could slow apoptotic processes, buying some extra time for the tracer to transport through the neurons while still maintaining tissue viability; alternatively, I thought that raising the temperature would increase rates of transport in the neurons, thereby shortening the time between dissociating the brain from its natural circulatory system and preserving the tissue in fixative. Normally, the brains were incubated at room temperature, which is around 20°C in our laboratory, but I also conducted experiments in which ice was used to bring the ACSF temperature down to about 15°C, or a heating plate was used to bring the ACSF temperature up to about 30°C.

2.8 Data collection and planned analysis

The following is a description of the data collection steps I performed, as well as the analysis steps I had planned to perform, all of which are applicable to a future

experiment in which sparse, and complete SBC labeling is achieved. Much of my time was spent at the confocal microscope, imaging labeled tissue samples in an effort to qualitatively describe the results of my various experiments. During an imaging session, if the quantity and quality of labeling looked promising, I collected image stacks and marked the files as a reminder to revisit them later for stitching and tracing. If, on the other hand, there were no labeled cells, or far too many, I did not spend time collecting any data, and instead took notes to describe the results.

Since the projection from the AVCN to the LSO is relatively long, I had to collect anywhere from 10 to 20 image stacks in order to completely capture the SBC somata and their terminal branches. Following the collection of these image stacks, the digital puzzle pieces had to be stitched back together into a montage of sorts. This step was necessary before the labeled axons could be traced and analyzed, so that the entire length of the neurons could be visualized at once. Stitching was accomplished with the Grid/Collection Stitching Plugin (Preibisch et al. 2009) in the open-source image processing software Fiji (Fiji is just ImageJ; Schindelin et al. 2012). In order for stitching to be successful, each image stack had to overlap slightly with its neighbouring stacks. While the path travelled by the labeled neurons was far from grid-like, collecting image stacks in a grid pattern was the only way I could get the stitching program to correctly align them afterwards.

Once the image stacks were stitched together, the tracing process could begin. While there are some automated tracing programs available, like the one included in the Neurolucida (MBF Bioscience) software suite, they never worked quite as well as the manual tracing plugin (Simple Neurite Tracer; Longair et al. 2011) that I spent the most

time with in Fiji. Automated tracing programs are built from complex algorithms that compare the brightness values of neighbouring pixels in a dataset, to determine whether those pixels likely form part of a continuous anatomical feature, like an axon. That may be an oversimplification of the matter, but the guiding principles of such programs are very similar to the strategies that human observers use when faced with similar tracing problems. That said, our capacity for learning and abstract thinking makes us more discerning and nuanced axon tracers than the current generation of automated tracing programs. Unsurprisingly, the success of either a human or computer in these situations depends greatly on the quality of the images in question. Namely, background fluorescence and inconsistency of cell fills can cause significant problems during tracing exercises. The background fluorescence was unfortunately quite high in the image samples I used to test the few automated tracing programs at my disposal. Therefore, when presented with my images of low signal-to-noise ratio, the automated tracing programs identified more false-positive axons than true ones. The time it would have taken to correct the mistakes made by the automated programs was better spent manually tracing the axons in the first place, which is what I did, until I encountered a problem that hindered further progress. For example, the fluorescent signal in the finer branches would often become too faint to be unambiguously distinguished from the background fluorescence. Other times, the background fluorescence itself would suddenly increase in an area where I expected to see more branches, indicating that those branches likely lysed before the tissue was fixed. Another problem occurred when two or more neighbouring cells were labeled, which was a frequent occurrence: Due to the tonotopic organization of

both the AVCN and the LSO, neighbouring cells in the former nucleus project to nearby areas in the latter, resulting in many overlapping axonal branches, and subsequent tracing difficulties.

Had I successfully traced an entire axonal arbour, the next steps would have been three-dimensional reconstruction and analysis. There are several measures I would have used to describe and quantify the anatomical refinement in this projection. In line with the anatomical refinement observed in the axonal arbours of the MNTB-LSO pathway (Sanes and Siverls 1991), and even in the dendritic arbours of LSO principal cells (Rietzel and Friauf 1998), we expected to see a tonotopic narrowing of the axonal arbours of the AVCN-LSO pathway. The most appropriate way to determine this would be to compare the width (measured parallel to the S-axis of the nucleus) and the total area of the LSO covered by axonal arbours of each age group. Those values would, of course, have to be normalized to the size of the entire LSO at each age, because the animals grow rapidly during the first three postnatal weeks. Comparing the number of branch points and terminal boutons across age groups would also provide valuable insight into the manifestation of anatomical refinement in these neurons. Furthermore, it would be interesting to quantify the dorsoventral (i.e. along the long axis of LSO bipolar neurons) spread of terminal boutons in this pathway (see Section 4.4, below).

3.0 Results

3.1 Parameterization #1: Location and direction of tracer application

Figure 2 (from Harrison and Irving 1965) depicts a schematic drawing of the rat CNC, along with some of the different labeling approaches I attempted. The rostrocaudal position of the microelectrode had a significant effect on the resulting quality of cell labeling. If the tracer was applied either too rostrally, or too caudally, SBCs were not likely to be labeled. That said, in all of my experiments, the majority of labeled cells were not SBCs, but rather GBCs. This was made evident by the circumvention of the LSO by most labeled axons (Figure 3). With regards to labeling SBCs, however, the best results were achieved by positioning the tip of the microelectrode approximately 20% of the length of the CNC caudal to the rostral pole (Figure 2).

The direction of approach used when applying the neuronal tracer also had an effect on the quality of cell labeling, but it did not affect the results as strongly as did the former manipulation. Approaching the nucleus rostrally rarely resulted in any SBCs being labeled, as noted by the lack of labeled axons leading to, or branching within the LSO. This is presumably due to the direction of tracer flow being directed caudally, towards GBCs and other cells types. Approaching the nucleus medially gave mixed results, and more care had to be taken to ensure that the tip of the microelectrode, and therefore the tracer itself, remained in the nucleus and did not cross through the lateral surface. Furthermore, granule cells in the superficial layer of the nucleus absorbed a significant amount of tracer in these experiments. Approaching the nucleus laterally gave the best, most consistent results. This is partly due to the maneuverability and visibility made possible by this approach, as well as the fact that the flow of tracer was directed along the long-axis (ventrolateral-dorsomedial) of the nucleus. Having tracer flow directed in this

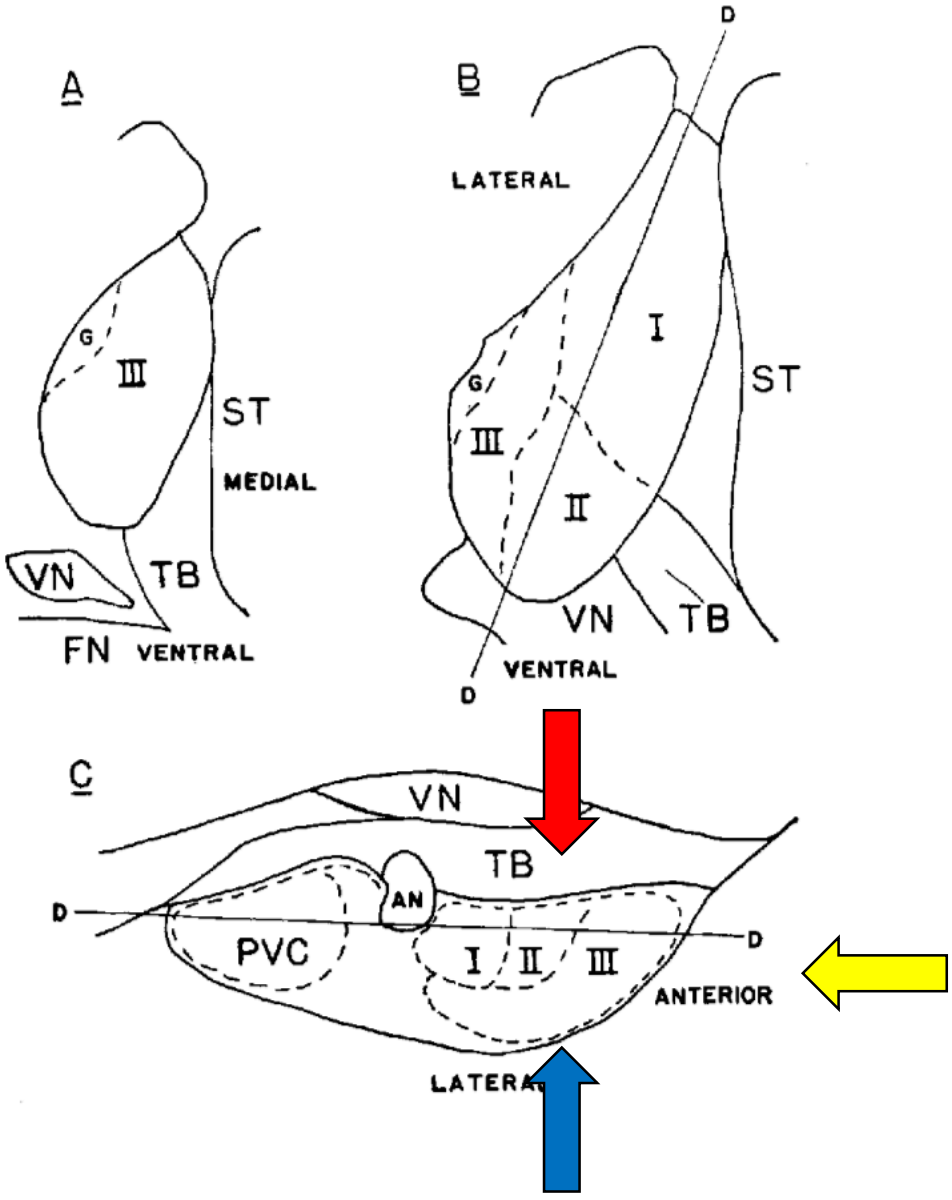

Figure 2. **Schematic drawing of the rat CNC (from Harrison and Irving 1965).** A) Transverse section through the rostral pole of the AVCN. B) Transverse section through the AVCN at the level of the red and blue arrows in Panel C. C) Horizontal section through the AVCN. The red arrow depicts the medial labeling approach; blue depicts lateral; and yellow depicts rostral.

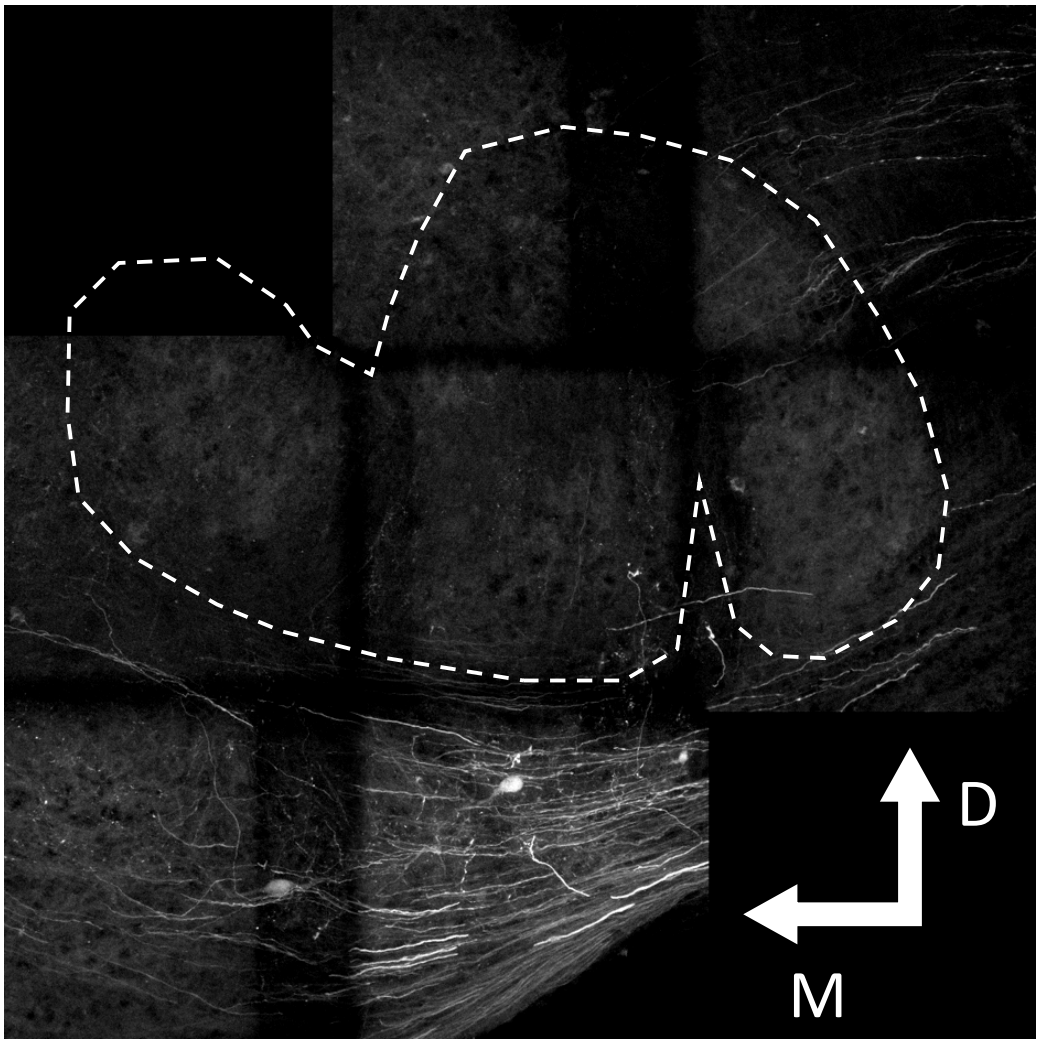

Figure 3. **Transverse section of P12 rat SOC.** Low magnification (20x objective) image of the axons labeled in the SOC following electroporation of micro-ruby in the AVCN (not seen). Note that most visible axons circumvent the LSO (dashed line).

plane increased the chances of labeling other SBCs, instead of more caudally lying GBCs.

3.2 Parameterization #2: Tracer selection

Biocytin was very easily taken up into both SBCs and GBCs (Figure 4), and transported quickly through the cells. Even in larger P21 brains, very short incubation times were required for the biocytin to be transported to the LSO, and even farther. Interestingly, biocytin was transported transsynaptically in some instances (Figure 5). In all cases, biocytin appeared to fill cells completely, labeling the most distant, fine axonal branches in the LSO. This tracer also labeled some fine dendritic processes in the AVCN. Unfortunately, significant levels of background fluorescence were observed in all experiments where biocytin was used as the tracer (Figure 6, inset).

Under normal conditions, neither Alexa488D nor micro-ruby were taken up easily by any cell type in the AVCN (Figure 7). Significant amounts of the tracers were present in cells only following electroporation. Alexa488D, being more than three times the size of micro-ruby, transported more slowly than the latter, and rarely reached the terminal branches in the LSO. When Alexa488D was seen in terminal branches within the LSO, there were too many labeled cells, and therefore axons, to clearly trace anything. The rate of transport of micro-ruby was between that of biocytin and Alexa488D, and was therefore seen in the terminal branches in the LSO much more frequently than Alexa488D. In all experiments using Alexa488D or micro-ruby, little to no background fluorescence was observed (Figure 8).

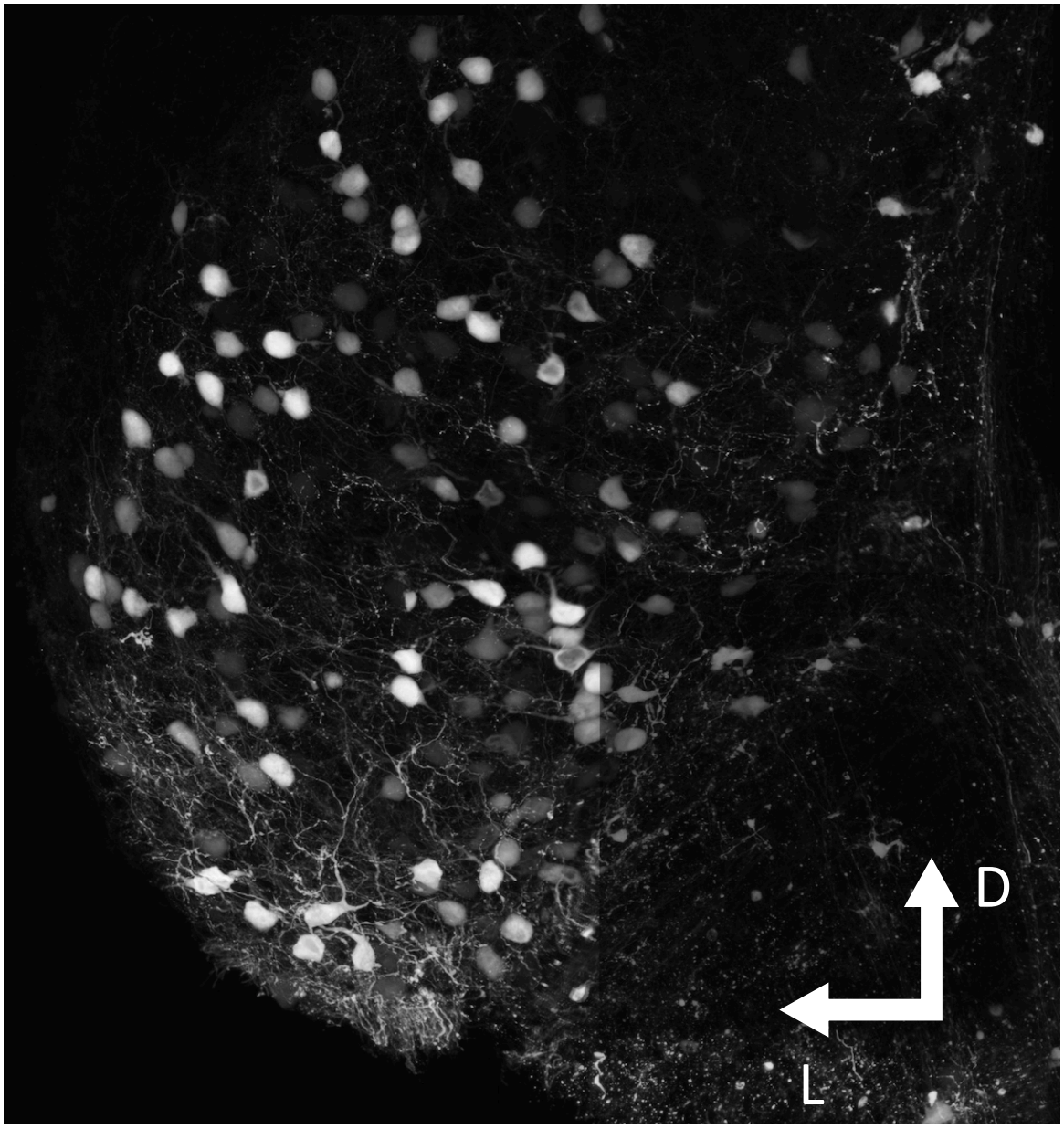

Figure 4. **Transverse section of P21 rat AVCN.** Low magnification (20x objective) image of the numerous cells labeled in the AVCN following the implantation of a crystal of biocytin. Note that most visible axons circumvent the LSO (dashed line).

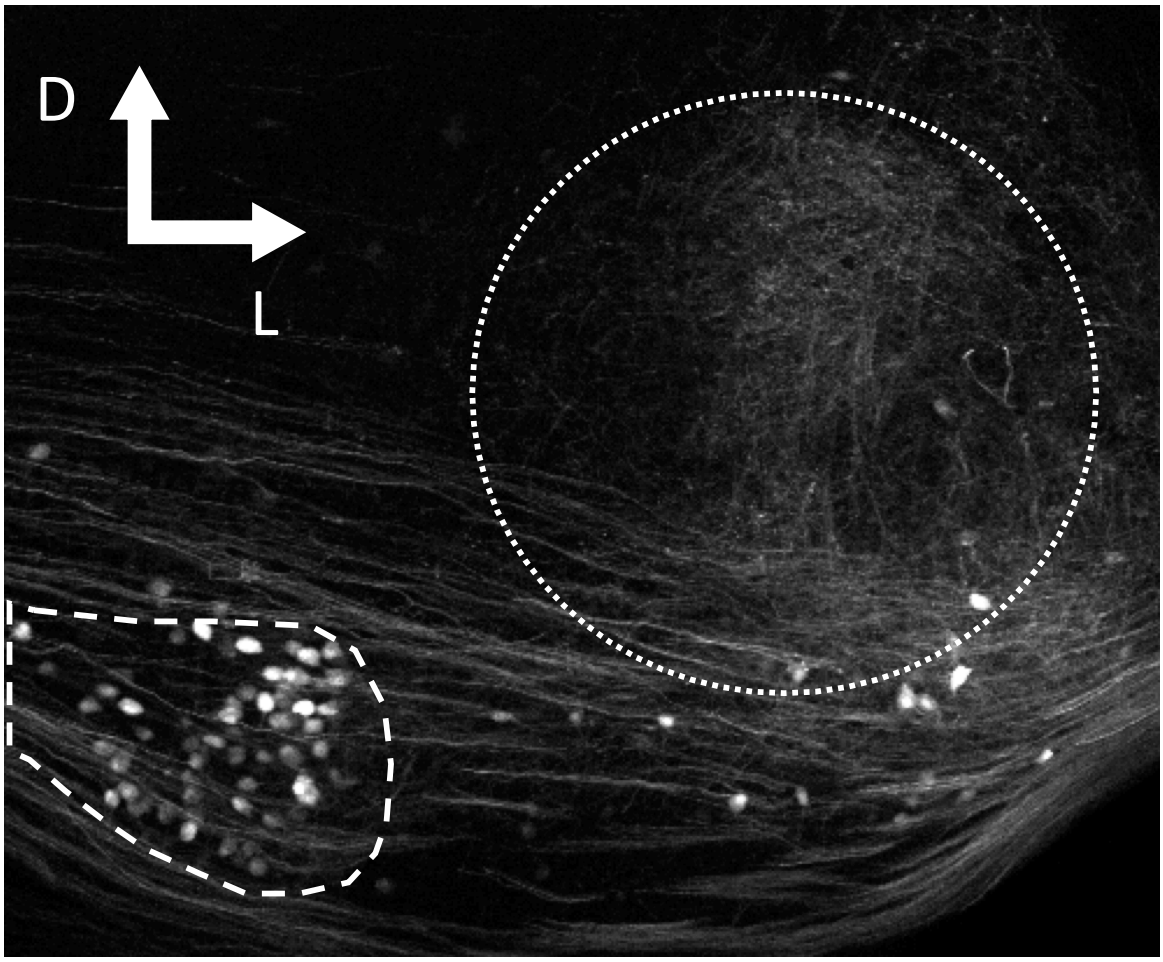

Figure 5. **Transverse section of P12 rat SOC.** Low magnification (20x objective) image of the many labeled axons in the SOC following bilateral implantations of biocytin crystals in the AVCNs. Although the LSO is not clearly visible, most labeled axons can still be seen bypassing the area where it would be located (dotted outline). Also note the cell bodies labeled transsynaptically in the MNTB (dashed outline).

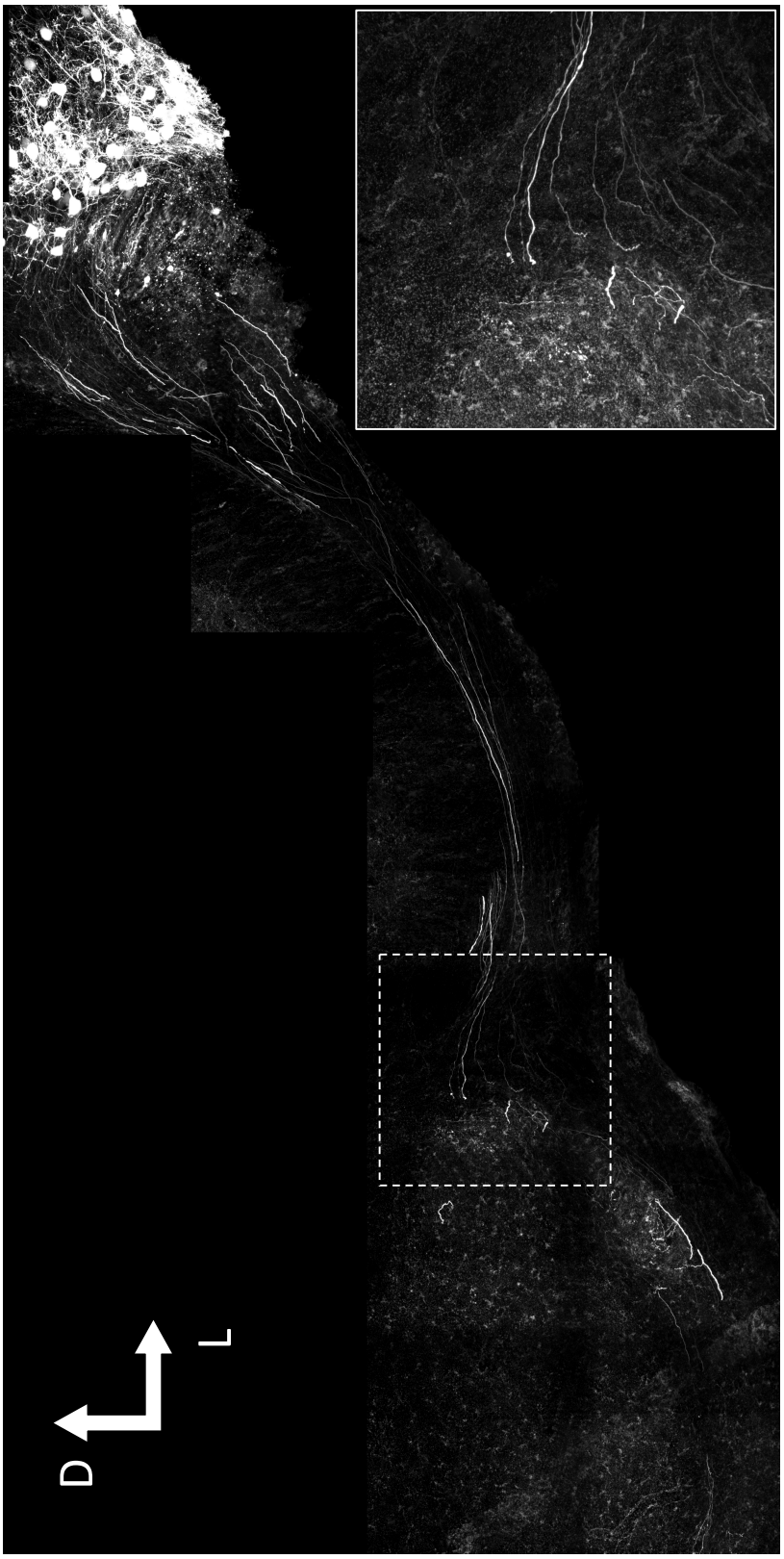

Figure 6. **Transverse section of P12 rat brainstem.** Montage of images tracing the AVCN-LSO pathway. The AVCN pictured here was pierced with the same microelectrode as the contralateral one (not seen), but with and no reapplication of biocytin crystals. Although the more dorsal part of the AVCN is not seen, there were no more labeled cells in that area. (Inset) Magnified image of the outlined area. Note the high levels of background fluorescence that obscure the labeled axons.

3.3 Parameterization #3: Tracer application method

Even using the smallest of crystals still just visible to the naked eye, implanting crystals of biocytin resulted in far too many labeled cells in the AVCN. This, in turn, led to far too many labeled axon terminals in the LSO to unequivocally trace a single arbour (Figure 9). The experiments in which I pierced the second AVCN of a brain, without reapplying biocytin to the electrode, resulted in fewer labeled cells in the AVCN, but still too many for successful tracing in the LSO (Figure 6).

Iontophoretically ejecting a biocytin solution (using the S48 stimulator) had the same effect as implanting solid crystals. Iontophoretically ejecting either Alexa488D or micro-ruby solutions, on the other hand, resulted in a cloud of tracer in the AVCN, with very little uptake into cells (Figure 7). Only with electroporation were cells of the AVCN labeled with the dextran tracers. Even then, however, labeling was inconsistent between successive experiments, resulting in either too many labeled cells or none at all. Interestingly, altering the electrical stimulating protocol had little to no effect on the consistency or quality of labeling.

Using the Neuroprobe intracellular amplifier in conjunction with the S48 stimulator resulted in more consistent labeling between experiments. Furthermore, the quality of labeling was closer to what would be required to fully trace an entire axonal arbour (Figure 8). That said, the number of cells labeled was still too great, or the labeling was incomplete.

Pressure-injecting dextran solutions had a similar effect to implanting solid crystals of biocytin. Evidently, the physical disturbance of the applied force was enough

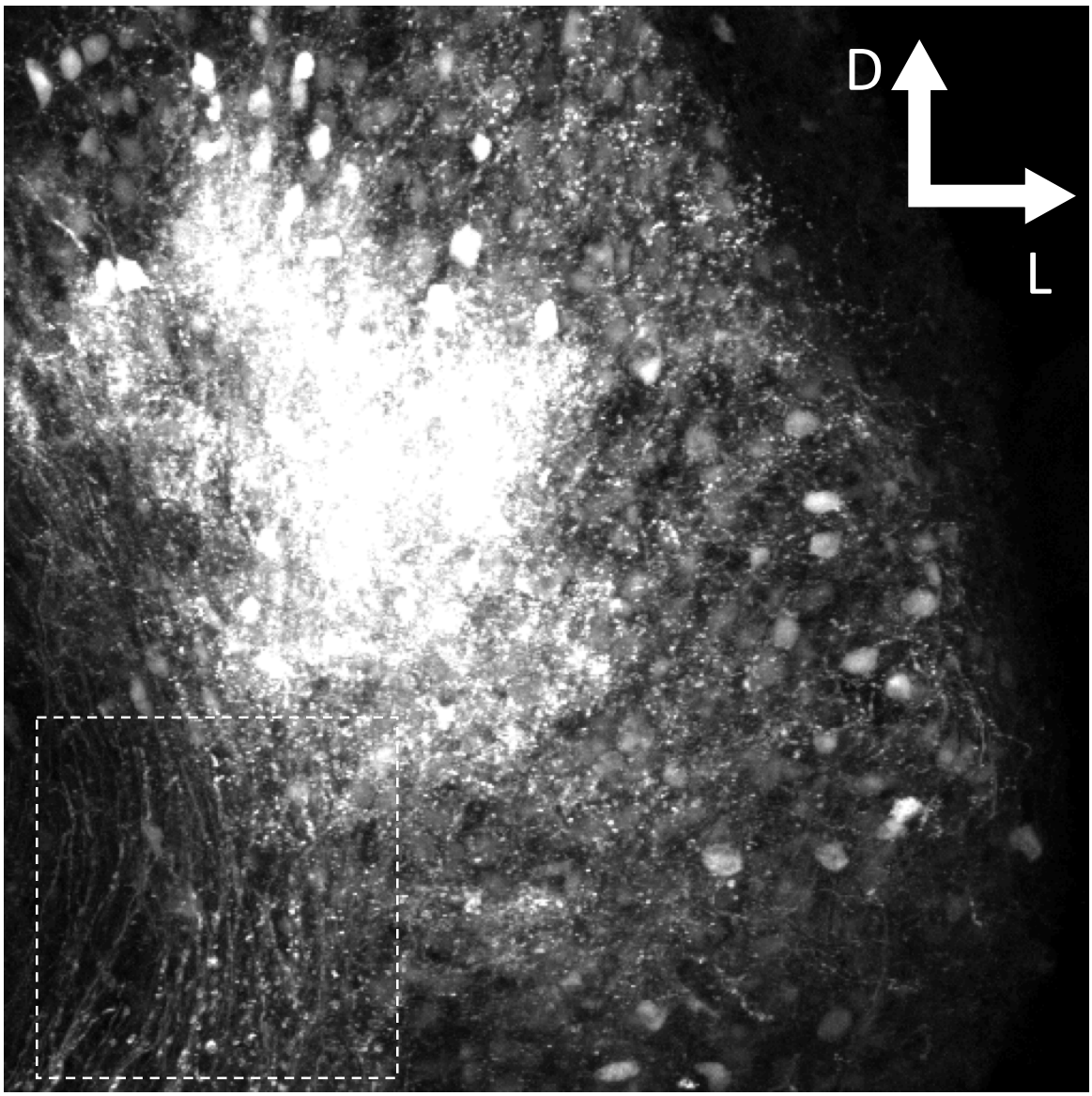

Figure 7. **Transverse section of P12 rat AVCN.** Cloud of tracer resulting from a pressure injection. Although some cell bodies around the periphery of the cloud are strongly labeled, no axons in any section of this brain were labeled more strongly than those seen in the dashed outline. Therefore, while axons were visible in the LSO (not seen), none were labeled strongly enough to enable successful tracing.

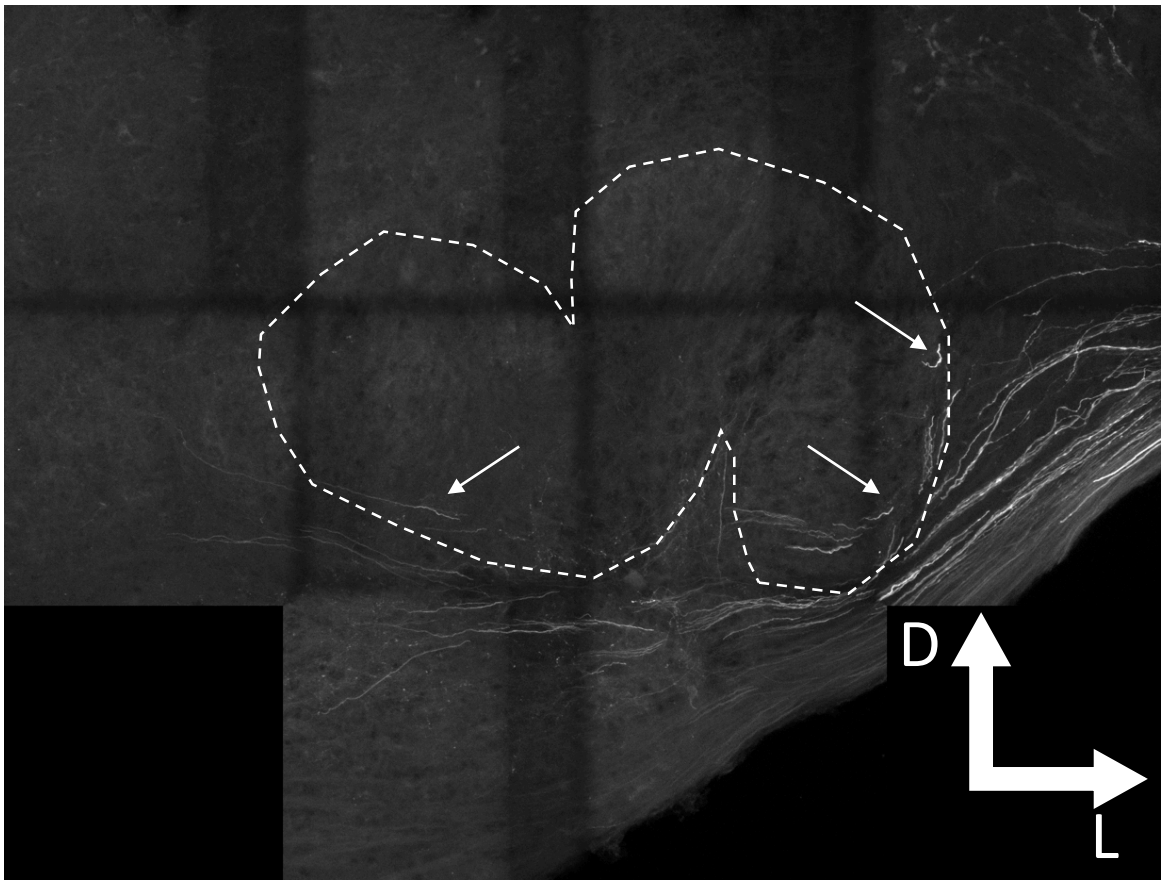

Figure 8. **Transverse section of P12 rat SOC.** Low magnification (20x objective) image of the labeling in the SOC resulting from electroporation of micro-ruby in the AVCN (not seen). Although many total axons are labeled, few (arrows) actually invade the LSO (dashed outline). Because the background fluorescence is so low when using this technique, the brightness of this image had to be increased in order to see the LSO.

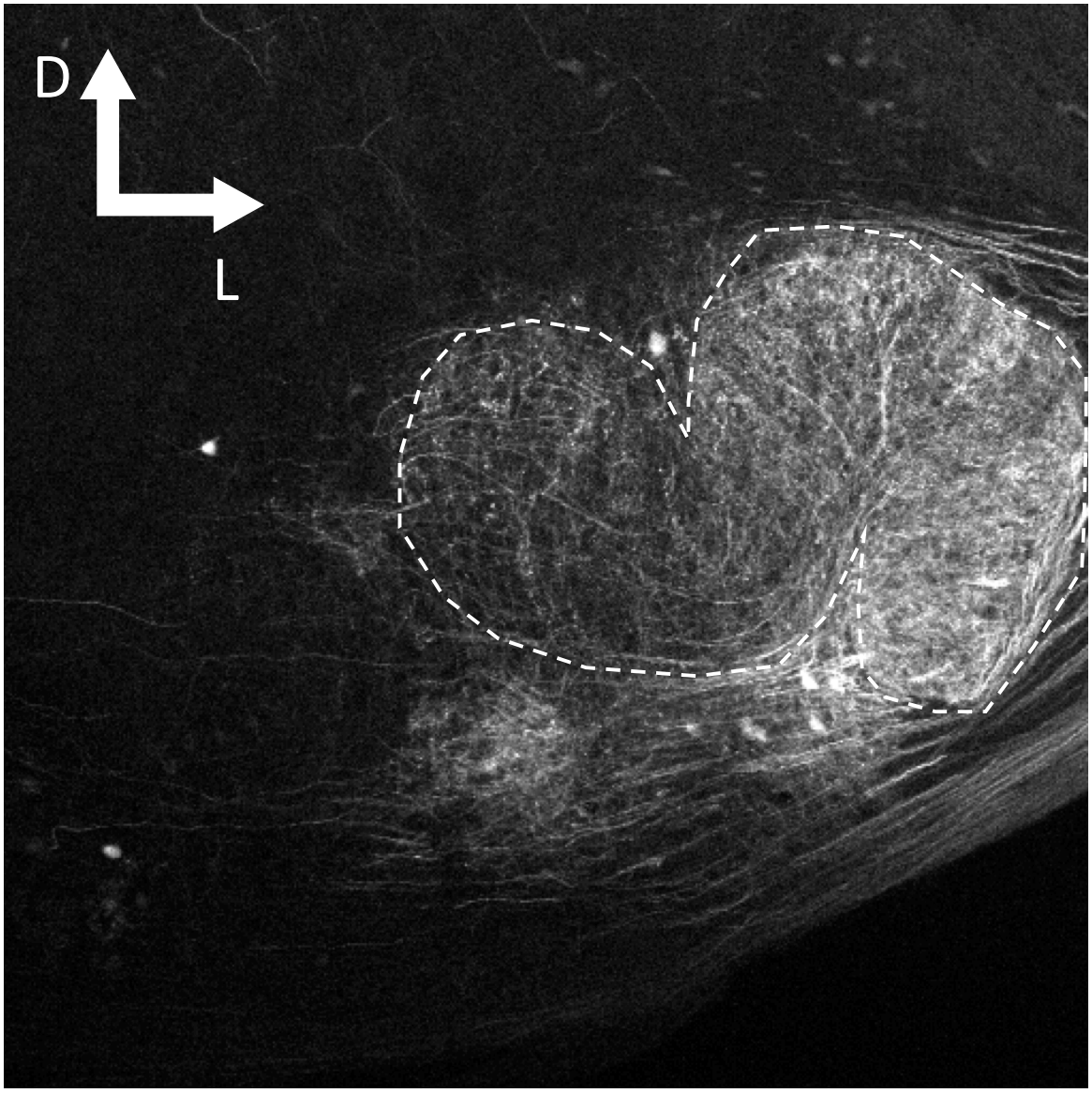

Figure 9. **Transverse section of P12 rat SOC.** Low magnification (20x objective) of the labeling in the SOC resulting from the implantation of a crystal of biocytin in the AVCN (not seen). Nearly the entire LSO (dashed outline) is visible due to the many labeled axons.

to destabilize the cell membranes long enough for tracer molecules to enter the somata. Following pressure-injections with electroporation improved the quality of labeling somewhat, yet still not to a point where a single axon could be traced in its entirety.

Finally, my attempts at reproducing the single-cell electroporation experiments of Rae and Levis (2001) were unsuccessful. That said, in my effort to achieve this level of precision, I was able to reduce the total number of cells labeled (including SBCs, GBCs, etc.) from hundreds (after implanting crystals of biocytin) to a few dozen (less than 10 of which were SBCs, on average).

3.4 Parameterization #4: Incubation times and conditions

Incubation times of four hours or less were only sufficient in experiments where biocytin was used as the tracer. In this timeframe, biocytin was not only able to reach the terminal branches of SBCs in the LSO, but also the terminal structures of GBCs (the calyces of Held) in the contralateral MNTB (Figure 10).

Because incubations never lasted more than four hours in biocytin experiments, tissue degradation was not an issue. The same cannot be said for experiments using Alexa488D or, to a lesser extent, micro-ruby. Alexa488D was never seen in the LSO following incubations of 3-4 hours, 4-5 hours, or even 5-6 hours. Even after incubation times of around seven hours, Alexa488D was rarely seen in the terminal axonal branches within the LSO. After such a long time in the *ex vivo* setup, the brain tissue became severely compromised. Neural debris could be seen floating in the ACSF bath, and upon transferring the brains from the bath to the vial containing fixative, I noted that the

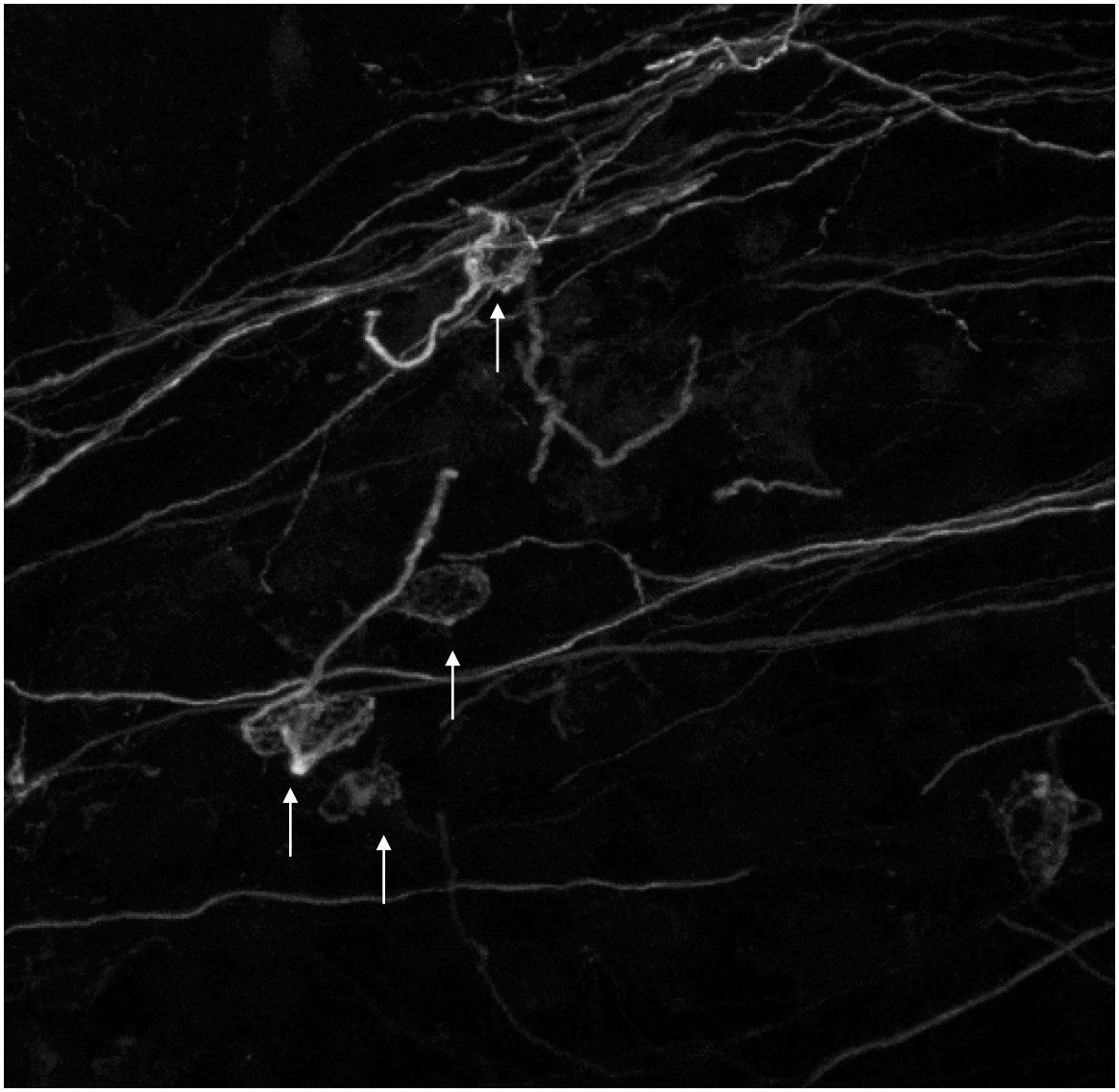

Figure 10. **Transverse section of P12 rat MNTB.** Calyces of Held (arrows) were visible in the MNTB following the implantation of a crystal of biocytin in the contralateral AVCN (not seen).

consistency of the brain tissue was markedly less rigid than before. When imaging tissue samples from brains incubated for 7-8 hours, there was a conspicuous lack of labeled cells in the AVCN, as well as a noticeably higher level of background fluorescence in the AVCN, the trapezoid body, and even the LSO. The increased background fluorescence was likely due to the leakage of tracer from dead or dying neurons that had been successfully labeled. When using micro-ruby, incubations lasting 4-5 hours were sufficient for younger (P12), smaller brains. In older (P21), larger brains, incubations of at least six hours were required in order for the micro-ruby to reach the terminal axonal branches in the LSO.

Manipulating the temperature of the ACSF bath did not improve the quality of cell labeling. Incubating the brains below room temperature, at about 15°C, did slow the rate of tissue degradation, as intended. In fact, incubations could be continued for up to nine hours without seeing any signs of large-scale tissue degradation. During this borrowed time, however, the tracer did not travel any farther than it had at room temperature (~20°C). Incidentally, the chemical and biological interactions governing tracer diffusion and transport were slowed as much as apoptotic processes were. Raising the bath temperature to ~30°C, closer to the temperature in which mammalian enzymes normally function (37°C), hastened apoptotic processes to such a degree that not a single uncompromised, labeled cell was observed upon imaging the tissue samples.

3.5 Summary table of results

Parameter changed/Technique used	Successful?	Main issue	Sample figures
Position of microelectrode too caudal	No	Few SBCs labeled	N/A
Rostral microelectrode approach	No	Few SBCs labeled	N/A
Medial microelectrode approach	No	Few SBCs labeled	N/A
Lateral microelectrode approach	Yes	N/A	All
Biocytin crystal implantation	No	Too many cells labeled	4, 5, 6, 9, 10
Alexa488D iontophoresis	No	Cells don't take up tracer	N/A
Alexa488D electroporation	No	Transport too slow	N/A
Micro-ruby iontophoresis	No	Cells don't take up tracer	3, 8
Micro-ruby electroporation	Yes	N/A	3, 8
Dextran pressure injection	No	Cells don't take up tracer	7
Incubate below room temperature	No	Transport too slow	N/A
Incubate above room temperature	No	Apoptosis too fast	N/A

Table 1. **Summary of results.**

4. Discussion

4.1 Tracer selection

Biocytin is an ideal tracer to use in living tissue for several reasons: 1) It is small and naturally occurring, and therefore relatively harmless as an exogenous substance; 2) it is readily taken up by neurons, making it unnecessary to strive for more technically difficult intracellular injections; and 3) it is actively and rapidly transported in the anterograde direction, making for short incubation times (McDonald 1992). Ironically, for many of the same reasons that it is considered to be so effective otherwise, biocytin was not the best choice of neuronal tracer in my experiments. The most significant issue was how easily biocytin was taken up into the cells. Even after months of practice, the average number of labeled cells in a 50 μm section still exceeded 20; consequently, the resulting number of labeled axon terminals in the LSO made tracing unfeasible. In several experiments, biocytin was even transported across synapses (Figure 5). This is problematic in a tracing study, because it is crucial to know where axons end and dendrites begin. A third problem resulted from the fact that biocytin and biotin are naturally occurring molecules. While the concentration of these molecules in labeled cell somata was much higher than in the surrounding tissue, the same could not be said for the most distal axonal branches. The concentration of tracer was more comparable to naturally occurring levels in these branches, and they were therefore obscured by background fluorescence. Unlike the blocking of nonspecific antibody-antigen interactions in immunohistochemistry experiments, I know of no way to limit the binding

of streptavidin to naturally occurring biotin without simply decreasing the concentration of the former – a manipulation that would also decrease the desired fluorescence signal. Therefore, applied extracellularly, biocytin was not a suitable tracer for my purposes. Injected intracellularly, on the other hand, it would most likely be the best option to answer my research question.

Dextrans are hydrophilic polysaccharides that are biologically inert due to an uncommon chemical structure that precludes enzymatic cleaving (Molecular Probes 2006). Depending on their size and associated chemical moieties, they can diffuse rapidly in both the anterograde and retrograde directions, and they can even be actively transported to some degree (Fritzsch 1993). This ability to be actively transported is, in fact, endowed by the addition of a biotin moiety. Applied extracellularly, cell labeling with dextrans was limited due to their inherent inability to cross cell membranes. The process of electroporation allows dextran molecules to enter neurons, and subsequently label their axons. Because the dextran molecules themselves are fluorescently tagged, no histological staining is required to make the labeled neurons visible, unlike biocytin. This eliminates the significant issue of high background staining in experiments using the latter tracer. Therefore, dextrans were the more suitable tracer to use for my purposes, given the techniques that I employed to label neurons.

4.2 Anterograde vs. retrograde tracing

While all three tracers I used can be transported retrogradely under different conditions or with slight modifications to their chemical structures, I only used them in an

anterograde fashion. There are many instances where retrograde tracing may be equally as useful as anterograde tracing – or perhaps even more so – in answering a particular research question, but this was not one. Since it would be nearly impossible to patch onto an axon terminal in the LSO and intracellularly inject a retrograde tracer, a larger injection of tracer would have to be made in the LSO in order for SBCs to be labeled. This would presumably result in a cloud of tracer extracellularly that would obscure the subsequent tracing of fine axonal branches, making this technique inappropriate to use in answering my research question. Alternatively, a retrogradely-transported transsynaptic tracer could be introduced into the contralateral or ipsilateral IC. This would eliminate the extracellular cloud of tracer in the LSO, as mentioned in the previous example. That said, this method would also be inadequate because there would be no way of knowing for certain whether all axon terminals of a single presynaptic neuron were labeled. This is because SBC axons terminate on more than one LSO cell, especially at younger ages, and so the possibility exists that some of those branches would not receive any tracer if the respective postsynaptic cells were unlabeled as well.

4.3 Labeling of SBCs vs. GBCs

As I alluded to in Section 3.1, whenever any cells in the AVCN were successfully labeled, the majority were GBCs. This was not made evident by the morphology of the cell somata and dendrites, but rather by the labeled axons projecting to the contralateral MNTB. In some experiments, the calyces of Held were even faintly labeled (Figure 10). While this is a purely anecdotal finding, it raises some interesting points. Based on the

position, angle, and depth of the microelectrode in all of my experiments, the majority of bushy cells in reach of the applied tracer should have been of the spherical variety; and yet, I consistently observed more staining in the axons of GBCs. The simplest explanation is that the applied tracer took the path of least resistance through the extracellular space towards more posterior parts of the AVCN, or even the anterior PVCN, where GBCs are more abundant. This most likely produced the higher levels of GBC axon staining that I observed, but there are alternative explanations. One possibility is that there are in fact more GBCs in the anterior part of the AVCN than previously thought. Another possibility is that the tracer molecules have an easier time entering GBCs than SBCs, so that even the relatively few GBCs in the anterior part of the AVCN take up proportionally more tracer than the more numerous SBCs. This second possibility, if true, would have some important implications for the functional differences between the two cell types; namely, it could be indicative of different membrane properties. Finally, it is worth mentioning that this incidental finding could be due to some combination of the three theories I proposed, for they are not mutually exclusive.

4.4 Functional role of LSO principal cell bipolar morphology

While bipolar cell morphology plays a clear functional role in MSO principal cells, by segregating the respective excitatory inputs from the two AVCNs, the same cannot be said for the similarly shaped cells of the LSO. LSO neurons only receive one excitatory input, which appears to be evenly distributed between both dendritic fields (Cant 1984). Although LSO principal cells do receive another large input, these

glycinergic axons from the MNTB fall on the cell somata (Cant 1984). So why do LSO neurons require two dendritic fields if there is no need to segregate the single excitatory input they receive? Cant (1984) made these observations based on ultrastructural electron micrographs, which is not to say they are incorrect, but it would be interesting to further explore the issue at a lower resolution and over the course of development. If we had found that SBC axon terminals are unequally distributed between the dorsal dendritic fields and the ventral ones, then it could have hinted at the functional role of LSO cell bipolar morphology.

4.5 Next steps and the implications of successful results

Due to the fact that my experiments precluded the tracing of a single axonal arbour, the most pertinent next step is to do just that. Given my exploration of the different techniques and parameters involved in extracellularly labeling SBCs, my conclusion is that the single-cell electroporation technique, used in conjunction with a low molecular weight dextran tracer, would be the most appropriate and efficient way of investigating anatomical refinement in the AVCN-LSO pathway.

I envision two possible outcomes for this future experiment: 1) Anatomical refinement in the AVCN-LSO pathway occurs at the same time as anatomical refinement in the MNTB-LSO pathway; or 2) refinement in one pathway precedes the other. Given the fact that functional refinement in the two pathways follows a similar timeline, it is fair to assume that anatomical refinement does as well, as per the first example. In this scenario, the respective processes of refinement in the two converging projections would

be independent of each other, but likely guided by the same principles. Were this not the case, however, and we found that refinement in one pathway precedes the other, then a different set of conclusions could be drawn. If one pathway were established first, and acted as a template for the other pathway, then the system would resemble the alignment of topographic maps that occurs in the mammalian superior colliculus (Triplett et al. 2009). In this circuit, the projection from the retinal ganglion cells is established first, via gradients of axon guidance molecules in both the projecting cells and the target nucleus. Following this, the projection from primary visual cortex aligns with the retinotopic map according to similar activity patterns exhibited between the two. Unlike in the LSO, both topographic projections converging on the superior colliculus are excitatory; this complicates matters for our model. Therefore, while the retinal-matching model of Triplett et al. (2009) might not be directly applicable to the LSO and its inputs, it is still interesting to consider.

4.6 Future avenues of research

Following the successful completion of this project, it would be interesting to perform the same experiments in the context of neonatal cochlear ablation. Just as Sanes and Takács (1993) described disturbed refinement in the inhibitory MNTB-LSO pathway following contralateral cochlear ablation, it would be informative to know the consequences of a complementary disturbance in the excitatory AVCN-LSO pathway. The conclusions of such an experiment would help uncover the relative contributions of spontaneous and sound-evoked activity to the process of anatomical refinement.

Something to consider before performing such an experiment, however, is the downstream degradation that occurs following cochlear ablation. Two days after unilateral cochlear ablation in P7 gerbils, there is already a 35% decrease in the number of neurons in the ipsilateral AVCN (Hashisaki and Rubel 1989). In the experiments of Sanes and Takács (1993), the degenerative effects of contralateral cochlear ablation on the LSO were, in a way, buffered by the extra synapse in the MNTB. The same would not be true for the experiment I am proposing, because the ipsilateral AVCN projects directly to the LSO. Degradation of the ipsilateral AVCN could have serious consequences for the integrity of the LSO. Such consequences could confound any measures of functional or anatomical refinement in the circuitry. A more suitable alternative, therefore, would be to selectively modify or disrupt the spontaneous activity in the circuitry, without irreversibly damaging the AVCN or any of its downstream nuclei. Thanks to work done by Tritsch et al. (2007), we know that spontaneous activity in the immature auditory system is initiated by an ATP-releasing, transient structure known at Kölliker's organ. While the idea of genetically altering ATP synthesizing or releasing machinery in these cells – in an effort to disrupt spontaneous activity – is tempting, it is important to remember that ATP is universally used in cells as a molecular energy source; accordingly, a disruption in ATP regulation could result in a host of unwanted consequences for affected cells. Therefore, until a more suitable, and viable alternative is found, cochlear ablation will have to suffice.

Another fascinating avenue of research would be to visualize and manipulate refinement in this circuitry in real-time. This could be accomplished in an organotypic

brainstem slice culture. Acute brain slices, for all their useful qualities, can only be maintained for relatively short periods of time *in vitro*. This precludes the investigation of any cellular processes with timecourses longer than an hour or two. Organotypic slice cultures, on the other hand, have been maintained for weeks at a time, allowing long-term processes to be studied (for review, see Gähwiler et al. 1997). In the rat, brainstem slices containing the CNC and the auditory nerve alone (Novozhilova et al. 2015), or the MNTB and LSO alone (Tong et al. 2010) have been successfully cultured for extended periods of time. To my knowledge, however, no one has successfully cultured a slice containing the AVCN, MNTB, and LSO. The difficulty with the rat auditory brainstem is that the various nuclei are not all found within the same transverse plane; namely, the AVCN is slightly more caudal than both the MNTB and the LSO. Therefore, it is challenging to slice the brain in such a way as to include both the MNTB and LSO, along with their respective inputs from the two AVCNs. Importantly, in the absence of input from the AVCN, the calyces of Held degenerate after 3 days *in vitro*, even while the brainstem slice itself remains viable for up to 28 days (Tong et al. 2010). To avoid severing any important neuronal projections, the brainstem could be sliced at an angle, but even then, the slice would have to be relatively thick. Unfortunately, thicker slices do not fare well in culture systems, because it is more difficult for the vital molecules in the culture medium and the perfusate to reach the centre of the tissue. While the successful implementation of this powerful technique would not come easily, to say the least, it is worth striving for nonetheless.

4.7 Summary

The unique circuitry of the auditory brainstem allows animals to localize sounds in their surrounding environments. In mammals, the LSO is the nucleus that computes ILDs, a binaural cue used to determine the origin of sounds along the azimuth. The LSO is excited by ipsilateral sounds, via the ipsilateral AVCN, and inhibited by contralateral sounds, via the ipsilateral MNTB, which is driven by the contralateral AVCN. The inputs to the LSO, and indeed the cells of the LSO itself, are organized tonotopically; that is to say, neighbouring cells respond best to neighbouring frequencies in the animal's audible range. Rough tonotopic organization is present during development, but the precision seen in mature circuits is only achieved through a process of refinement that occurs during the first few postnatal weeks in rats. Refinement occurs in two phases: first, functional refinement, in which most synapses are eliminated, while the remaining ones are strengthened; and then, anatomical refinement, in which axonal arbours become more confined to a single isofrequency band. Functional and anatomical refinement have been thoroughly investigated in the MNTB-LSO pathway. In the AVCN-LSO pathway, on the other hand, only functional refinement has been explored.

Over the course of approximately two years, I conducted a number of different experiments, all with the same goal: to characterize the timeline and extent of anatomical refinement in the AVCN-LSO pathway. In all of my experiments, I attempted to anterogradely label a very small number of SBCs in the AVCN, and trace them all the way to their axonal arbours in the ipsilateral LSO. My time in the laboratory was spent learning, testing, and troubleshooting the various techniques I employed to this end. In

pursuit of the best possible results, I explored several different neuronal tracers, along with different ways of applying each tracer, and different incubation times and conditions. While intracellular injections would undoubtedly provide a satisfactory answer to this research question, I do not believe it is necessary to strive for such a technically challenging labeling method. Given my exploration of this parameter space, I have concluded that an extracellular labeling approach is sufficient to fully label and trace SBCs projecting from the AVCN to the LSO, and, further, that the single-cell electroporation method, with a dextran tracer like micro-ruby, is the most appropriate technique to use going forward.

4.8 Concluding remarks

Questions of circuit development and refinement are ubiquitous in the field of neuroscience: How do developing axons navigate the complex geography of the nervous system in search of their final targets? Why do neural circuits require some fine-tuning after their initial setup, and how is this accomplished? How do circuits repair themselves, or compensate otherwise, following an injury? On the very surface, these big-picture questions may seem relatively straight-forward, but delving into the specifics of each unique circuit complicates matters exponentially. For example, here is a simple enough answer to the first question: axon guidance molecules. Given a particular circuit, however, any number of different guidance molecules can be expressed in various spatial and temporal patterns, and their very functions can change depending on where (in the nervous system) or when (during development) they bind to one of their possibly

numerous receptors. With a staggering number of unique circuits in the mammalian nervous system alone, trying to unveil their various mechanisms of development and refinement seems like a masochistic endeavour. One could argue, however, that questions of this nature are what define neuroscience; for what is a nervous system if not plastic? And so, answering these critical questions is of the utmost importance in an effort to chip away at the higher-order questions in the field.

To this end, neural plasticity has been studied in countless circuits, across numerous species, and at different developmental stages within those species. Ask any neuroscientist to provide an example of neural plasticity, however, and the answer will almost always be the same: NMDA receptor-mediated long-term potentiation, one of the most well-studied, and therefore most well-understood, forms of plasticity. While this is by no means an incorrect answer, the frequency with which it occurs is disproportionate to its biological relevance. This example is just one of perhaps several types of plasticity found at one particular synapse (CA3-CA1) in a relatively small part of the brain (the hippocampus). My point is not to diminish the significance of this classic model, but rather to draw attention to the fact that the phenomenon of neural plasticity is a vastly heterogeneous one with no single prototypical example. For years, interest in the unique MNTB-LSO pathway has forced research into the AVCN-LSO pathway onto the backburner. There is nothing unique about the latter pathway itself, aside from the fact that it aligns with the former; why waste time investigating the plasticity and refinement that occur here, if they most likely resemble the analogous processes that occur in the well-studied topographic maps of the visual system, for example? The fact that two

different synapses share certain characteristics does not necessarily mean that plasticity at those synapses is governed by similar rules, or expressed in a similar manner. Accordingly, the refinement of the AVCN-LSO pathway cannot be generalized to the refinement of another excitatory projection in a different sensory system, or even another excitatory projection in the auditory system, let alone the MNTB-LSO projection. The act of generalization in biology is a double-edged sword; while it is convenient, and even appropriate at times, to lump phenomena together under uniting rules, there are always caveats and outright exceptions to those rules. That is not to say that the AVCN-LSO pathway is necessarily an outlier in this respect. In fact, I believe that the rules governing plasticity and anatomical refinement in this pathway will surprise no one, once conclusively determined. Unfortunately, with regards to advancing the field, speculation and personal opinions are no substitute for scientifically-supported facts. Therefore, the mystery that is anatomical refinement in the AVCN-LSO pathway remains unsolved – for now.

References

Auffarth B. 2013. Understanding smell – the olfactory stimulus problem. Neurosci Biobehav Rev 37(8):1667–1679.

Balakrishnan V, Becker M, Löhrke S, Nothwang HG, Güresir E, Friauf E. 2003. Expression and function of chloride transporters during development of inhibitory neurotransmission in the auditory brainstem. J Neurosci 23(10):4134–4145.

Barker M, Billups B, Hamann M. 2009. Focal macromolecule delivery in neuronal tissue using simultaneous pressure ejection and local electroporation. J Neurosci Methods 177(2):273–284.

Becker M, Nothwang HG, Friauf E. 2003. Differential expression pattern of chloride transporters NCC, NKCC2, KCC1, KCC3, KCC4, and AE3 in the developing rat auditory brainstem. Cell Tissue Res 312(2):155–165.

Blaesse P, Ehrhardt S, Friauf E, Nothwang H. 2005. Developmental pattern of three vesicular glutamate transporters in the rat superior olivary complex. Cell Tissue Res 320(1):33–50.

Blatchley BJ, Cooper WA, Coleman JR. 1987. Development of auditory brainstem response to tone pip stimuli in the rat. Brain Res 429(1):75–84.

Bledsoe SC Jr, Snead CR, Helfert RH, Prasad V, Wenthold RJ, Altschuler RA. 1990. Immunocytochemical and lesion studies support the hypothesis that the projection from the medial nucleus of the trapezoid body to the lateral superior olive is glycinergic. Brain Res 517(1-2):189–194.

Boudreau JC, Tsuchitani C. 1968. Binaural interaction in the cat superior olive S segment. J Neurophysiol 31(3):442–454.

Brawer JR, Morest DK, Kane EC. 1974. The neuronal architecture of the cochlear nucleus of the cat. J Comp Neurol 155(3):251–300.

Brown MC, Santos-Sacchi J. 2008. Fundamental neuroscience. 3rd ed. Squire LR, Berg D, Bloom FE, du Lac S, Ghosh A, Spitzer NC, editors. Burlington, MA: Academic Press. Audition; p 609–636.

Burger RM, Cramer KS, Pfeiffer JD, Rubel EW. 2005. Avian superior olivary nucleus provides divergent inhibitory input to parallel auditory pathways. J Comp Neurol 481(1):6–18.

Cant NB. 1984. The fine structure of the lateral superior olivary nucleus of the cat. J Comp Neurol 227(1):63–77.

Cant NB, Benson CG. 2003. Parallel auditory pathways: projection patterns of the different neuronal populations in the dorsal and ventral cochlear nuclei. Brain Res Bull 60(5-6):457–474.

Cant NB, Casseday JH. 1986. Projections from the anteroventral cochlear nucleus to the lateral and medial superior olivary nuclei. J Comp Neurol 247(4):457–76.

Case D, Gillespie DC. 2011. Pre- and postsynaptic properties of glutamatergic transmission in the immature inhibitory MNTB-LSO pathway. J Neurophysiol 106(5):2570–9.

Case D, Zhao X, Gillespie DC. 2011. Functional refinement in the projection from ventral cochlear nucleus to lateral superior olive precedes hearing onset in rat. PLoS One 6(6):e20756.

Chen X, Gabitto M, Peng Y, Ryba NJP, Zuker CS. 2011. A gustotopic map of taste qualities in the mammalian brain. Science 333(6047):1262–1266.

Clause A, Kim G, Sonntag M, Weisz CC, Vetter D, Rubsamen R, Kandler K. 2014. The precise temporal pattern of prehearing spontaneous activity is necessary for tonotopic map refinement. Neuron 82:822–835.

Cramer KS. 2005. Eph proteins and the assembly of auditory circuits. Hear Res 206(1-2):42–51.

Ehmann H, Salzig C, Lang P, Friauf E, Nothwang HG. 2008. Minimal sex differences in gene expression in the rat superior olivary complex. Hear Res 245:65–72.

Ehrlich I, Löhrke S, Friauf E. 1999. Shift from depolarizing to hyperpolarizing glycine action in rat auditory neurones is due to age-dependent Cl^- regulation. J Physiol 520(1):121–137.

Escoffre JM, Portet T, Wasungu L, Teissié J, Dean D, Rols MP. 2009. What is (still not) known of the mechanism by which electroporation mediates gene transfer and expression in cells and tissues. Mol Biotechnol 41(3):286–295.

Ford MC, Grothe B, Klug A. 2009. Fenestration of the calyx of Held occurs sequentially along the tonotopic axis, is influenced by afferent activity, and facilitates glutamate clearance. J Comp Neurol 514(1):92–106.

Fremeau RT, Burman J, Qureshi T, Tran CH, Proctor J, Johnson J, Zhang H, Sulzer D, Copenhagen DR, Storm-Mathisen J, et al. 2002. The identification of vesicular glutamate transporter 3 suggests novel modes of signaling by glutamate. Proc Natl Acad Sci U.S.A. 99(22):14488–14493.

Friauf E. 1992. Tonotopic order in the adult and developing auditory system of the rat as shown by c-fos immunocytochemistry. Eur J Neurosci 4(9):798–812.

Friauf E. 1993. Transient appearance of calbindin-D28k-positive neurons in the superior olivary complex of developing rats. J Comp Neurol 334(1):59–74.

Fritzsch B. 1993. Fast axonal diffusion of 3000 molecular weight dextran amines. J Neurosci Methods 50(1):95–103.

Gähwiler BH, Capogna M, Debanne D, McKinney RA, Thompson SM. 1997. Organotypic slice cultures: a technique has come of age. Trends Neurosci 20(10):471–477.

Galli L, Maffei L. 1988. Spontaneous impulse activity of rat retinal ganglion cells in prenatal life. Science 242(4875):90–91.

Gillespie DC, Kim G, Kandler K. 2005. Inhibitory synapses in the developing auditory system are glutamatergic. Nat Neurosci 8(3):332–8.

Glendenning KK, Baker BN, Hutson KA, Masterton RB. 1992. Acoustic chiasm V: inhibition and excitation in the ipsilateral and contralateral projections of LSO. J Comp Neurol 319(1):100–122.

Glendenning KK, Masterton RB. 1983. Acoustic chiasm: efferent projections of the lateral superior olive. J Neurosci 3(8):1521–1537.

Glendenning KK, Masterton RB, Baker BN, Wenthold RJ. 1991. Acoustic chiasm III: nature, distribution, and sources of afferents to the lateral superior olive in the cat. J Comp Neurol 310(1):377–400.

Grothe B, Pecka M, McAlpine D. 2010. Mechanisms of sound localization in mammals. Physiol Rev 90(3):983–1012.

Guinan JJ, Li RY. 1990. Signal processing in brainstem auditory neurons which receive giant endings (calyces of Held) in the medial nucleus of the trapezoid body of the cat. Hear Res 49(1-3):321–334.

Gummer AW, Mark RF. 1994. Patterned neural activity in brain stem auditory areas of a prehearing mammal, the tammar wallaby (Macropus eugenii). Neuroreport 5:685–688.

Haas K, Jensen K, Sin WC, Foa L, Cline HT. 2002. Targeted electroporation in Xenopus tadpoles in vivo – from single cells to the entire brain. Differentiation 70(4-5):148–154.

Hackney CM, Osen KK, Kolston J. 1990. Anatomy of the cochlear nuclear complex of guinea pig. Anat Embryol 182(2):123–149.

Hackney CM, Pick GF. 1986. The distribution of spherical cells in the anteroventral cochlear nucleus of the guinea pig. Brit J Audiol 20:215–220.

Harrison JM, Irving R. 1965. The anterior ventral cochlear nucleus. J Comp Neurol 124:15–41.

Harrison JM, Irving R. 1966a. Ascending connections of the anterior ventral cochlear nucleus in the rat. J Comp Neurol 126(1):51–63.

Harrison JM, Irving R. 1966b. The organization of the posterior ventral cochlear nucleus in the rat. J Comp Neurol 126(3):391–401.

Harrison JM, Irving R. 1966c. Visual and nonvisual auditory systems in mammals. Science 154(3750):738–743.

Harrison JM, Warr WB. 1962. A study of the cochlear nuclei and ascending auditory pathways of the medulla. J Comp Neurol 119:341–379.

Hashisaki GT, Rubel EW. 1989. Effects of unilateral cochlea removal on anteroventral cochlear nucleus neurons in developing gerbils. J Comp Neurol 283:465–73.

Helfert RH, Schwartz IR. 1986. Morphological evidence for the existence of multiple neuronal classes in the cat lateral superior olivary nucleus. J Comp Neurol 244(4):533–549.

Helfert RH, Schwartz IR. 1987. Morphological features of five neuronal classes in the gerbil lateral superior olive. Am J Anat 179(1):55–69.

Hudspeth AJ. 2013. Principles of neural science. 5th ed. Kandel ER, Schwartz JH, Jessell TM, Siegelbaum SA, Hudspeth AJ, editors. New York: McGraw-Hill. The inner ear; p 654–681.

Ito T, Oliver DL. 2010. Origins of glutamatergic terminals in the inferior colliculus identified by retrograde transport and expression of VGLUT1 and VGLUT2 genes. Front Neuroanat 4:135

Kandler K, Friauf E. 1993. Pre- and postnatal development of efferent connections of the cochlear nucleus in the rat. J Comp Neurol 328(2):161–84.

Kandler K, Friauf E. 1995. Development of glycinergic and glutamatergic synaptic transmission in the auditory brainstem of perinatal rats. J Neurosci 15(10):6890–6904.

Kandler K, Gillespie DC. 2005. Developmental refinement of inhibitory sound-localization circuits. Trends Neurosci. 28(6):290–6.

Killackey HP, Rhoades RW, Bennett-Clarke CA. 1995. The formation of a cortical somatotopic map. Trends Neurosci 18(9):402–407.

Kim G, Kandler K. 2003. Elimination and strengthening of glycinergic/GABAergic connections during tonotopic map formation. Nat Neurosci 6(3):282–90.

Kim G, Kandler K. 2010. Synaptic changes underlying the strengthening of GABA/glycinergic connections in the developing lateral superior olive. Neuroscience 171(3):924–933.

Kitzes LM, Kageyama GH, Semple MN, Kil J. 1995. Development of ectopic projections from the ventral cochlear nucleus to the superior olivary complex induced by neonatal ablation of the contralateral cochlea. J Comp Neurol 353(3):341–63.

Kotak VC, Korada S, Schwartz IR, Sanes DH. 1998. A developmental shift from GABAergic to glycinergic transmission in the central auditory system. J Neurosci 18(12):4646–4655.

Kullmann PHM, Ene FA, Kandler K. 2002. Glycinergic and GABAergic calcium responses in the developing lateral superior olive. Eur J Neurosci 15(7):1093–1104.

Kullmann PHM, Kandler K. 2001. Glycinergic/GABAergic synapses in the lateral superior olive are excitatory in neonatal C57Bl/6J mice. Dev Brain Res 131(1-2):143–147.

Lippe WR. 1994. Rhythmic spontaneous activity in the developing avian auditory system. J Neurosci 14:1486–1495.

Löhrke S, Srinivasan G, Oberhofer M, Doncheva E, Friauf E. 2005. Shift from depolarizing to hyperpolarizing glycine action occurs at different perinatal ages in superior olivary complex nuclei. Eur J Neurosci 22(11):2708–2722.

Longair MH, Baker DA, Armstrong JD. 2011. Simple neurite tracer: open source software for reconstruction, visualization and analysis of neuronal processes. Bioinformatics 27(17):2453–2454.

Luo F, Wang Q, Farid N, Liu X, Yan J. 2009. Three-dimensional tonotopic organization of the C57 mouse cochlear nucleus. Hear Res 257(1-2):75–82.

Luo L, Flanagan JG. 2007. Development of continuous and discrete neural maps. Neuron 56(2):284–300.

Maffei L, Galli-Resta L. 1990. Correlation in discharges of neighboring rat retinal ganglion cells during prenatal life. Proc Natl Acad Sci U.S.A. 87(7):2861–2864.

Masterton B, Diamond IT, Harrison JM, Beecher MD. 1967. Medial Superior Olive and Sound Localization. Science 155(3770):1696–1697.

Masterton B, Thompson GC, Bechtold JK, RoBards MJ. 1975. Neuroanatomical basis of binaural phase-difference analysis for sound localization: a comparative study. J Comp Physiol Psychol 89(5):379–386.

Meister M, Wong RO, Baylor DA, Shatz CJ. 1991. Synchronous bursts of action potentials in ganglion cells of the developing mammalian retina. Science 252(5008):939–943.

Molecular Probes. 2006 Apr 5. Dextran conjugates. <https://www.lifetechnologies.com/order/catalog/product/D7162>. Accessed 2015 Aug 12.

Moore MJ, Caspary DM. 1983. Strychnine blocks binaural inhibition in lateral superior olivary neurons. J Neurosci 3(1):237–242.

Nabekura J, Katsurabayashi S, Kakazu Y, Shibata S, Matsubara A, Jinno S, Mizoguchi Y, Sasaki A, Ishibashi H. 2004. Developmental switch from GABA to glycine release in single central synaptic terminals. Nat Neurosci 7(1):17–23.

Novozhilova E, Englund-Johansson U, Kale A, Jiao Y, Olivius P. 2015. Effects of ROCK inhibitor Y27632 and EGFR inhibitor PD168393 on human neural precursors co-cultured with rat auditory brainstem explant. Neuroscience 287:43–54.

Osen KK. 1969. Cytoarchitecture of the cochlear nuclei in the cat. J. Comp. Neurol. 136(4):453–484.

Preibisch S, Saalfeld S, Tomancak P. 2009. Globally optimal stitching of tiled 3D microscopic image acquisitions. Bioinformatics 25(11):1463–1465.

Rae JL, Levis RA. 2001. Single-cell electroporation. Eur J Physiol 443:664–670.

Ramón y Cajal S. 1909. Histologie du système nerveux du l'homme et des vertébrés. Volume 1, Généralités, moelle, ganglions rachidiens, bulbe & protubérance. Azoulay L, translator. Paris: Maloine. 986 p. Translation of: Textura del sistema nervioso del hombre y de los vertebrados.

Rietzel H-J, Friauf E. 1998. Neuron types in the rat lateral superior olive and developmental changes in the complexity of their dendritic arbors. J Comp Neurol 390:20–40.

Saenz M, Langers DRM. 2014. Tonotopic mapping of human auditory cortex. Hear Res 307:42–52.

Saint Marie RL, Ostapoff EM, Morest DK, Wenthold RJ. 1989. Glycine-immunoreactive projection of the cat lateral superior olive: possible role in midbrain ear dominance. J Comp Neurol 279(3):382–396.

Sanes DH, Geary WA, Wooten GF, Rubel EW. 1987. Quantitative distribution of the glycine receptor in the auditory brain stem of the gerbil. J Neurosci 7(11):3793–3802.

Sanes DH, Siverls V. 1991. Development and specificity of inhibitory terminal arborizations in the central nervous system. J Neurobiol 22(8):837–854.

Sanes DH, Takács C. 1993. Activity-dependent refinement of inhibitory connections. Eur J Neurosci 5:570–574.

Schindelin J, Arganda-Carreras I, Frise E, Kaynig V, Longair M, Pietzsch T, Preibisch S, Rueden C, Saalfeld S, Schmid B, et al. 2012. Fiji: an open-source platform for biological-image analysis. Nat Methods 9(7):676–682.

Shatz CJ, Stryker MP. 1988. Prenatal tetrodotoxin infusion blocks segregation of retinogeniculate afferents. Science 242(4875):87–89.

Smith PH, Joris PX, Carney LH, Yin TC. 1991. Projections of physiologically characterized globular bushy cell axons from the cochlear nucleus of the cat. J Comp Neurol 304(3):387–407.

Sperry RW. 1963. Chemoaffinity in the orderly growth of nerve fiber patterns and connections. Proc Natl Acad Sci U.S.A. 50:703–710.

Tollin DJ. 2003. The lateral superior olive: a functional role in sound source localization. Neuroscientist 9(2):127–143.

Tong H, Steinert JR, Robinson SW, Chernova T, Read DJ, Oliver DL, Forsythe ID. 2010. Regulation of Kv channel expression and neuronal excitability in rat medial nucleus of the trapezoid body maintained in organotypic culture. J Physiol 588(9):1451–1468.

Triplett JW, Owens MT, Yamada J, Lemke G, Cang J, Stryker MP, Feldheim DA. 2009. Retinal input instructs alignment of visual topographic maps. Cell 139(1):175–85.

Tritsch NX, Yi E, Gale JE, Glowatzki E, Bergles DE. 2007. The origin of spontaneous activity in the developing auditory system. Nature 450(7166):50–5.

Webster DB, Trune DR. 1982. Cochlear nuclear complex of mice. Am J Anat 163(2):103–30.

Wong RO, Meister M, Shatz CJ. 1993. Transient period of correlated bursting activity during development of the mammalian retina. Neuron 11(5):923–38.

Yin TC, Chan JC. 1990. Interaural time sensitivity in medial superior olive of cat. J Neurophysiol 64(2):465–488.